Journal of Atmospheric and Solar-Terrestrial Physics 143-144 (2016) 71–87

Contents lists available at ScienceDirect

Journal of Atmospheric and Solar-Terrestrial Physics

journal homepage: www.elsevier.com/locate/jastp

Variability of mesospheric water vapor above Bern in relation to the 27-day solar rotation cycle

Martin Lainer [a,*], Klemens Hocke [a,b], Niklaus Kämpfer [a,b]

[a] Institute of Applied Physics, University of Bern, Bern, Switzerland
[b] Oeschger Center for Climate Change Research, University of Bern, Bern, Switzerland

ARTICLE INFO

Article history:
Received 4 November 2015
Received in revised form
3 March 2016
Accepted 23 March 2016
Available online 29 March 2016

Keywords:
Mesospheric water vapor
Solar Lyman-α flux
Solar rotation cycle
Atmospheric variability

ABSTRACT

Many studies investigated solar–terrestrial responses (thermal state, O_3, OH, H_2O) with emphasis on the tropical upper atmosphere. In this paper the focus is switched to water vapor in the mesosphere at a mid-latitudinal location. Eight years of water vapor profile measurements above Bern (46.88°N/7.46°E) are investigated to study oscillations with the focus on periods between 10 and 50 days. Different spectral analyses revealed prominent features in the 27-day oscillation band, which are enhanced in the upper mesosphere (above 0.1 hPa, ~64 km) during the rising sunspot activity of solar cycle 24. Local as well as zonal mean Aura MLS observations support these results by showing a similar behavior. The relationship between mesospheric water and the solar Lyman-α flux is studied by comparing the similarity of their temporal oscillations. The H_2O oscillation is negatively correlated to solar Lyman-α oscillation with a correlation coefficient of up to −0.3 to −0.4, and the phase lag is 6–10 days at 0.04 hPa. The confidence level of the correlation is ≥99%. This finding supports the assumption that the 27-day oscillation in Lyman-α causes a periodical photodissociation loss in mesospheric water. Wavelet power spectra, cross-wavelet transform and wavelet coherence analysis (WTC) complete our study. More periods of high common wavelet power of H_2O and solar Lyman-α are present when amplitudes of the Lyman-α flux increase. Since this is not a measure of physical correlation a more detailed view on WTC is necessary, where significant (two sigma level) correlations occur intermittently in the 27 and 13-day band with variable phase lock behavior. Large Lyman-α oscillations appeared after the solar superstorm in July 2012 and the H_2O oscillations show a well pronounced anti-correlation. The competition between advective transport and photodissociation loss of mesospheric water vapor may explain the sometimes variable phase relationship of mesospheric H_2O and solar Lyman-α oscillations. Generally, the WTC analysis indicates that solar variability causes observable photochemical and dynamical processes in the mid-latitude mesosphere.

1. Introduction

The middle atmosphere plays an important role in earth's climate through coupling processes with the troposphere. On a short time scale a coupling can be induced by propagation, absorption and reflection of planetary waves, whereas the influence of stratospheric warmings or the change in eddy-mean flow interactions by e.g. ENSO (El Niño-Southern Oscillation), QBO (Quasi-biennial Oscillation) or solar variability act on longer intra-seasonal to inter-annual time scales. The mesosphere and stratosphere are considerably affected by the energy input from the sun, mainly due to absorption of solar radiation by ozone and oxygen. Mesospheric altitudes range between ~50 km (stratopause) and ~80–85 km (mesopause) and the temperature decreases with altitude. The polar mesosphere undergoes large seasonal changes in dynamics and composition. Large seasonal temperature extremes occur between the summer and winter pole. Due to an intense dynamical forcing, the temperature changes in the mesosphere are reversed to that expected from direct solar forcing. Temperatures below 150 K at the summertime polar mesopause region allow the formation of ice clouds, known as Polar Mesospheric Clouds (PMC). Since their formation is directly related to temperature and the abundance of water vapor they can serve as an indicator for global change (Thomas, 1996).

In general, the mesosphere is dominated by radiative equilibrium and the breakdown of local thermal equilibrium (non-LTE) in case of rotational transition is more a subject in the transition region to the thermosphere and above (>90 km).

In previous work (e.g., Hood, 2013), it is studied how the stratosphere responds to the 27-day solar rotation cycle and the

* Corresponding author.
E-mail address: martin.lainer@iap.unibe.ch (M. Lainer).

http://dx.doi.org/10.1016/j.jastp.2016.03.008

11-year solar cycle. Solar variability can change ozone concentrations through direct photodissociation loss or secondary induced chemical reactions with e.g. the radical family (HO_x, NO_x, ClO_x, BrO_x) and thereby modify temperature and dynamics in the middle atmosphere and more far-reaching the net energy budget of the troposphere. The existence of high amounts of stratospheric ozone is explained with photochemical reactions, the so-called Chapman cycle (Eq. (1a–d)) (Chapman, 1930)

$$O_2 + h\nu \longrightarrow O + O \quad (1a)$$

$$O + O_2 + M \longrightarrow O_3 + M \quad (1b)$$

$$O + O_3 \longrightarrow 2O_2 \quad (1c)$$

$$O_3 + h\nu \longrightarrow O_2 + O \quad (1d)$$

The MLT (Mesosphere and Lower Thermosphere) is the region where the energy input from the sun can be deposited through photodissociation of atmospheric constituents like O_2, O_3, CH_4 or H_2O by solar Lyman-α radiation at a wavelength of 121.56 nm. However this is possible down to the lower mesosphere or even upper stratosphere owing to a low absorption cross-section of molecular oxygen in this short wavelength region (cf. Brasseur and Solomon, 2006). As shown by Chabrillat and Kockarts (1997) model predictions of Lyman-α photodissociation rates depend on the parametrization of O_2 absorption cross-sections. Compared to the approximation of a constant O_2 cross-section σ, they used a newly developed parametrization based on high spectral measurements of σ at Lyman-α and involving a temperature dependency e.g. raised the water vapor loss rates in the mesosphere by up to 10% with respect to prior model results.

Whilst there is an increasing interest in understanding the impact of small scale natural processes or variability on the earth's atmosphere, we present measurements of mesospheric water vapor above Bern by microwave radiometry since April 2007 in view of oscillations on time scales between 10 and 50 days. Based on different analysis methods for geophysical time series, such as digital band-pass filtering, Welch's Method (Welch, 1967) for estimating the power spectral density or the cross wavelet transform and wavelet coherence (Grinsted et al., 2004) to find common features in two different data time series, we discuss whether the observed recurring H_2O oscillations can be related to solar irradiance perturbations in the 121.56 nm spectral line of hydrogen (Lyman-α).

Besides the major 11-year solar cycle due to magnetic activity, a mean synodical period of 27.28 days is prominent which originates from the sun rotation. The accompanying drive-by (drift) of sun spots, starting from in-homogeneous magnetic field patterns on the sun surface, triggers the irradiance oscillation. Linking mechanism between mesospheric water vapor and solar radiation at short wavelengths is of interest. Photolysis of water vapor typically happens by reactions like

$$H_2O + h\nu \longrightarrow H + OH \quad (2)$$

$$H_2O + h\nu \longrightarrow H_2 + O(^1D) \quad (3)$$

When a photodissociation process happens, the probability of the reaction channels is 75% for the first (Eq. (2)) and 25% for the second one (Eq. (3)) (Stief et al., 1972). Vardavas et al. (1998) investigated the impact of H_2O photolysis by solar Lyman-α on the ozone concentration above 0.04 hPa, which is equivalent to an altitude of 70 km. The production of hydrogen affects the ozone minimum observed in the upper mesosphere. These findings underline an important influence of the Lyman-α flux on the chemical composition of the upper atmosphere.

In addition to photochemical reactions, dynamical processes can affect the abundance of H_2O. Many studies contributed to the understanding of waves in the middle atmosphere with periods of 2 days (Salby, 1981; Yue et al., 2012), 5 days (Wu et al., 1994; Riggin et al., 2006), and 16 days (McDonald et al., 2011; Scheiben et al., 2014). A few papers considered variations from 20 days up to three months (Wu and Jiang, 2005; Mayr et al., 2009; Studer et al., 2012). The focus has been on mesospheric wind and temperature (1.7–3 months periods, Mayr et al., 2009), the variability in diurnal tides of H_2O, O_3 and gravity wave patterns (inter-annual to seasonal periods, Wu and Jiang, 2005) or on stratospheric ozone (10–60 day periods, Studer et al., 2012).

Signatures of the 27-day variability of the sun were found in tropical OH and H_2O measurements in the mesosphere from the space-borne MLS (Microwave Limb Sounder) instrument on the Aura satellite (Shapiro et al., 2012). They detected maximal positive correlation coefficients of 0.79 for OH and negative coefficients of -0.74 for H_2O. Additionally the amplitude of the normalized power spectra of OH and H_2O are significantly higher during a high solar activity period (2004–2005 compared to 2008–2009), suggesting that solar variability controls to some extent the observed intensity of OH and H_2O oscillations in the mesosphere. A much longer time period of observations, altogether 8 years starting from 2007-04-01, which are alike to Shapiro et al. (2012) divided into a high and low solar activity period (each 4 years, hereafter denoted as reference period A and B), is the basis of our study in this paper, what quantitatively strengthens the statistical results.

Moreover, Ruzmaikin et al. (2014) correlated middle atmospheric CO (zonally averaged) as measured by Aura MLS in the time span 2004–2012 to solar UV variability on the sun rotation time scale. By using a wavelet coherence method, an intermittent 27-day recurring signal has been identified near the mesopause.

There is a lack of scientific studies dedicated to mid-latitudinal measurements of chemical compounds and their response to short as well as long-term solar variability. A focus had been put on the tropical upper atmosphere, extra-tropical parts in combination with water vapor found less attention, motivating the current study to search for solar signals in mesospheric water vapor as observed by a ground-based microwave radiometer. A higher influence of internal atmospheric disturbances (e.g. planetary waves, gravity waves or SSWs) on the amount of mesospheric H_2O has to be considered in the mid-latitudes. Planetary waves, also known as Rossby waves, play a key role in describing atmospheric dynamics. Due to their vertical structure a distinction between barotropic and baroclinic Rossby waves is common (Holton and Hakim, 2013). A numerical investigation by Krivolutsky et al. (2003) showed that oscillations in solar UV radiation due to the solar rotational cycle can trigger propagating Rossby waves in the middle atmosphere by a resonant feedback with a period of 25–27 days. Such studies and theories inspired our research, but a thorough and broad analysis is needed to reveal how the Lyman-α variations correlate to the amount of water vapor observed. First we describe the processed data of mesospheric H_2O measured at Bern by a ground-based microwave remote sensing instrument (Section 2.1) and solar irradiance data from a space-borne instrument (Section 2.2). Section 3 is dedicated to different data analysis and filtering methods, whereas Sections 4 and 5 present the outcome of our investigations, followed by a discussion (Section 6) and conclusions (Section 7).

2. The data

2.1. Ground-based microwave radiometry of H_2O

Ground-based microwave radiometry offers the possibility to continuously measure concentrations of atmospheric trace gases at altitudes between roughly 30 and 80 km and is therefore an excellent method for studying the middle atmosphere.

The Middle Atmospheric Water Vapor Radiometer (MIAWARA) has been developed at the Institute of Applied Physics at the University of Bern (Switzerland) and measures the emission of the pressure broadened rotational transition line emerging from water vapor molecules at a center frequency of 22.235 GHz (Kämpfer et al., 2012). The measured spectra are used to retrieve water vapor profiles by means of radiative transfer calculations and the Optimal Estimation Method (Rodgers, 2000) with use of the retrieval software package ARTS/qpack (Eriksson et al., 2005, 2011). As rotational transitions are not affected by non-LTE up to the mesopause we can use the Planck function for a source term. The water vapor signal from the middle atmosphere is weak, which makes it unavoidable to increase the signal to noise ratio by integrating the spectra. This study uses a MIAWARA profile retrieval with a constant integration time of calibrated and balanced spectra of 72 h. An overall spectrum bandwidth of 100 MHz is processed. The a priori profile information is taken from a monthly mean zonal mean climatology using Aura MLS version 2.2 data from 2004 to 2008. MLS version 4.2 data are used to initialize pressure, temperature and geopotential height as PTZ source in the retrieval calculations. MIAWARA is continuously operating on the roof of the building for Atmospheric Remote Sensing in Zimmerwald (46.88°N/7.46°E, 907 m amsl) close to Bern since September 2006 and delivers data to NDACC (Network for the Detection of Atmospheric Composition Change). The vertical resolution of the instrument varies between 11 km in the stratosphere and 14 km in the mesosphere (Deuber et al., 2005). The water vapor product from Aura MLS has a vertical resolution between 1.3–3.6 km from 316–0.22 hPa and degrades to 6–11 km for pressures levels above 0.22 hPa (Livesey et al., 2015). We note, in the mesosphere MLS has at least a 20% better vertical resolution than the MIAWARA instrument. By comparing mean amplitude spectra of the water vapor time series from MLS and MIAWARA we apply a convolution of the MLS observations with the averaging kernels from MIAWARA to account for the differences in the vertical resolution.

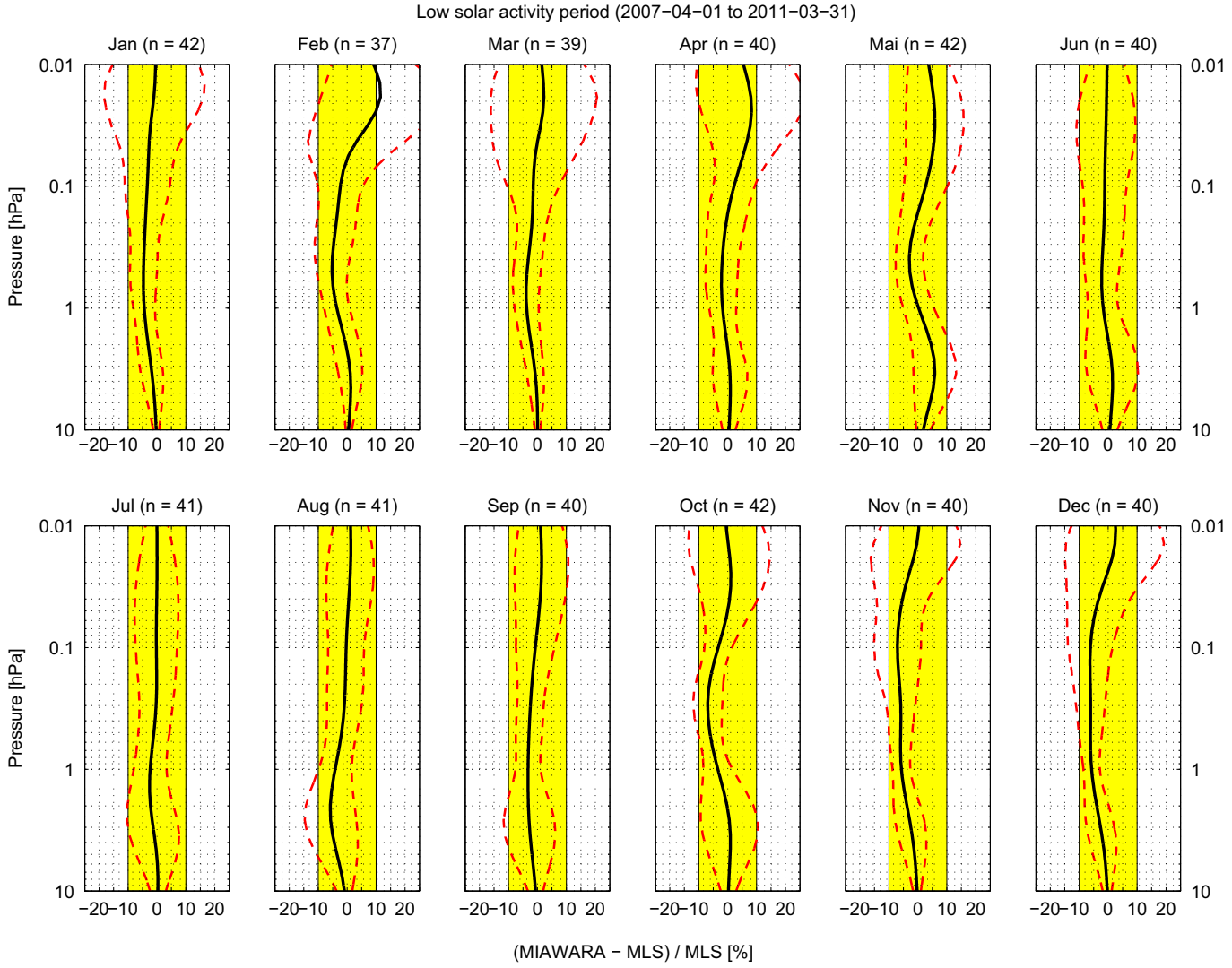

Fig. 1. Monthly mean relative differences (black lines) of the water vapor difference profiles between MIAWARA and Aura MLS v4.2. The mean difference profiles are calculated from measurements in the period from 2007-04-01 until 2011-03-31. The number of individual profiles considered per month is given by *n*. Dashed red lines show the standard deviations $\pm\sigma$ and the yellow stripes indicate the ±10% areas. (For interpretation of the references to color in this figure caption, the reader is referred to the web version of this paper.)

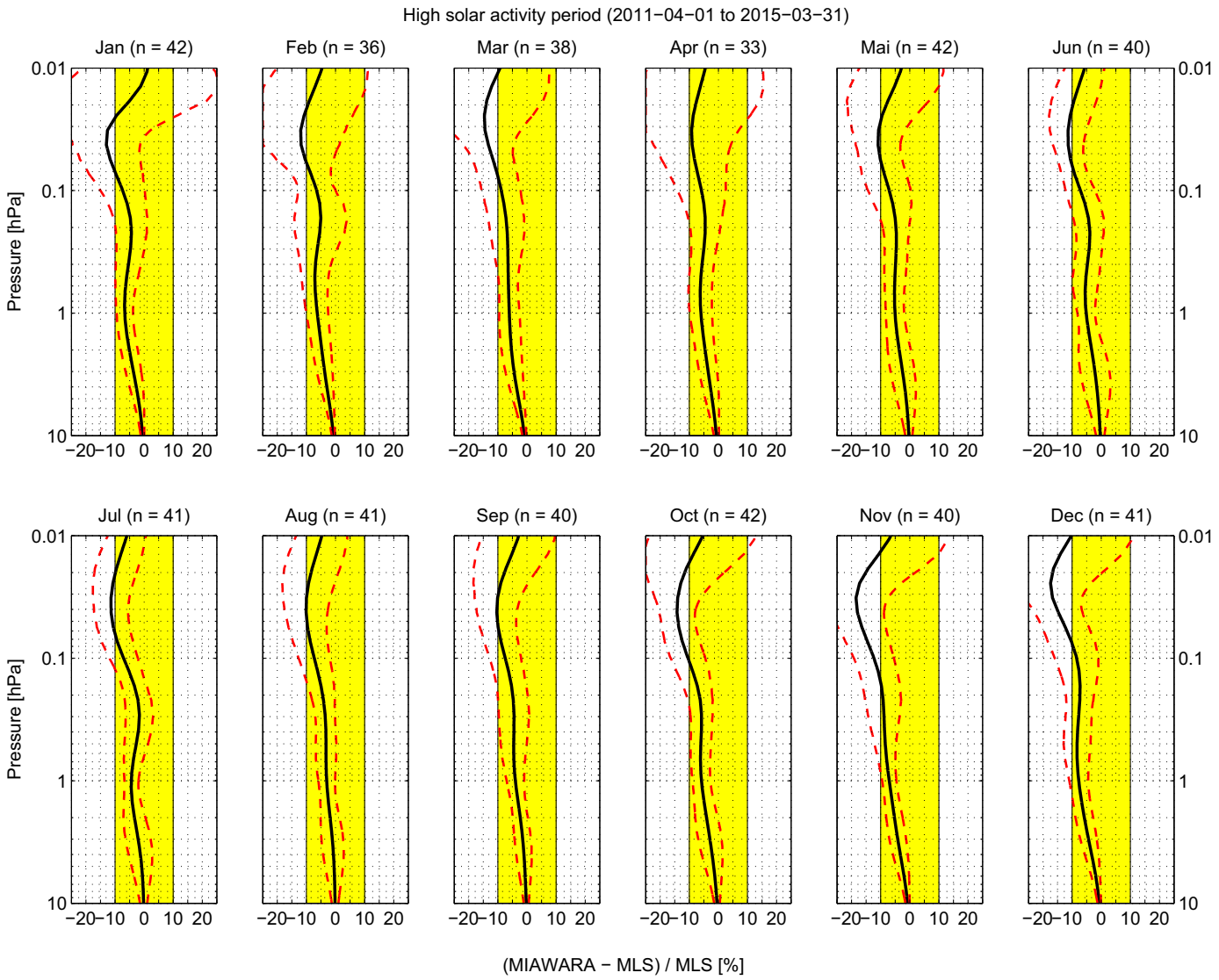

Fig. 2. Same as Fig. 1, except for the time period from 2011-04-01 until 2015-03-31.

A monthly mean profile comparison between MIAWARA and Aura MLS v4.2 is shown in Fig. 1 (reference period A) and Fig. 2 (reference period B). Mostly the absolute relative difference between 10 and 0.01 hPa is below 5% (Fig. 1). In bounded altitude regions some months reveal that the relative difference are slightly higher, but they rarely exceed 10%. The mean profiles in Fig. 2 show that below 0.1 hPa the results are comparable to period A. In the upper mesosphere higher biases are present, on occasion during winter months, for instance in November and December. There Aura MLS measures higher H_2O mixing ratios in the mean (up to about 15%). For both period cases A and B the standard deviations clearly increase in the upper mesosphere (above 0.1 hPa).

With a sufficient long integration time of the spectra it is possible to measure H_2O mixing ratios from 10 to 0.01 hPa since the Acousto-Optical Spectrometer (AOS) has been replaced by a digital FFT (Fast Fourier-Transform) Spectrometer in March 2007. However, only since October 2010 it is possible to get H_2O profiles with a measurement response greater than 0.6 up to ~0.01 hPa with the setting of constant 72 h integration due to hard- and software updates. A faster stepper motor for the mirror was installed and an adjustment of the calibration cycle took place. In consequence the effective measurement time of the H_2O line increased and vice versa the measurement noise dropped.

We define an upper mean measurement limit for reference period A (2007-04-01 to 2011-03-31) and B (2011-04-01 to 2015-03-31) as the mean pressure level where the a priori contribution is below 0.4. As Fig. 3 shows, these limits are 0.027 hPa(≈ 73 km) and 0.011 hPa(≈ 79 km).

2.2. Irradiance of solar Lyman-α

For linking and correlating the water vapor observations from MIAWARA with solar data we use the latter obtained from the LASP (Laboratory for Atmospheric and Space Physics) Interactive Solar IRradiance Data Center (LISIRD) website. They provide a wide range of solar spectral observations from the XUV to the NIR and advanced total solar irradiance measurements. Data gaps are filled with data from irradiance models. The composite Lyman-α time series (April 2007–March 2015) uses measurements from the Solar Radiation and Climate Experiment (SORCE) mission (Anderson and Cahalan, 2005; Rottman, 2005), the Thermosphere Ionosphere Mesosphere Energetics and Dynamics (TIMED) SEE (solar EUV

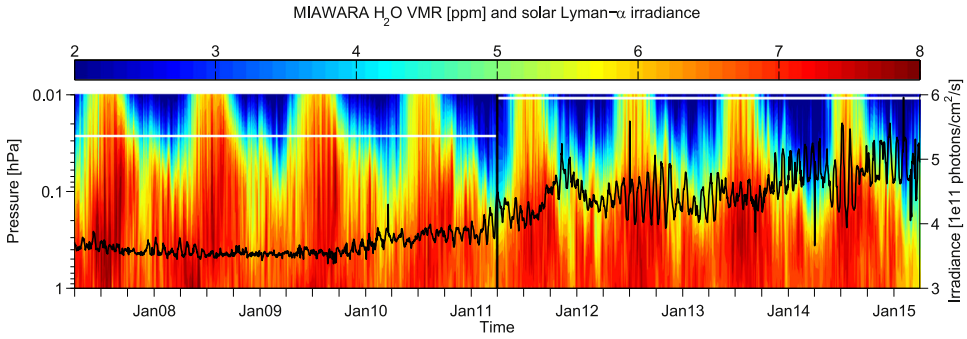

Fig. 3. Geophysical time series of water vapor from the ground-based microwave radiometer MIAWARA close to Bern (contour plot) and combined solar Lyman-α irradiance (overlapped black line plot) data from SORCE, TIMED SEE and earlier missions and models. The vertical black line separates the period of the defined high (right side) and low (left side) activity of solar Lyman-α oscillations. Horizontal white lines indicate the mean upper measurement limits of 0.027 hPa (2007-04-01 to 2011-03-31) and 0.011 hPa (2011-04-01 to 2015-03-31).

experiment) mission (Woods et al., 1998) and results from irradiance model simulations. As outlined by Woods et al. (2000) TIMED and SORCE data are used since 2003 and scaled to match the UARS (Upper Atmosphere Research Satellite) measurements reference level. The data product from SORCE is associated to the Solar Stellar Irradiance Comparison Experiment (SOLSTICE), which measures solar spectral radiance in the range 115–320 nm. The spectral resolution of the space-borne instrument is on the order of 0.1 nm and a check of accuracy revealed errors to be in general below 5% (McClintock et al., 2000).

3. Statistical data analysis methods

3.1. Band-pass filtering analysis

A digital non-recursive FIR (Finite Impulse Response) band-pass filter with a Hamming window is applied to MIAWARA and Aura MLS mesospheric water vapor measurements and to the solar Lyman-α time series to derive mean absolute wave amplitude spectra and the time evolution of the relative amplitude of the 27-day oscillation. The numerical set-up of the band-pass filter

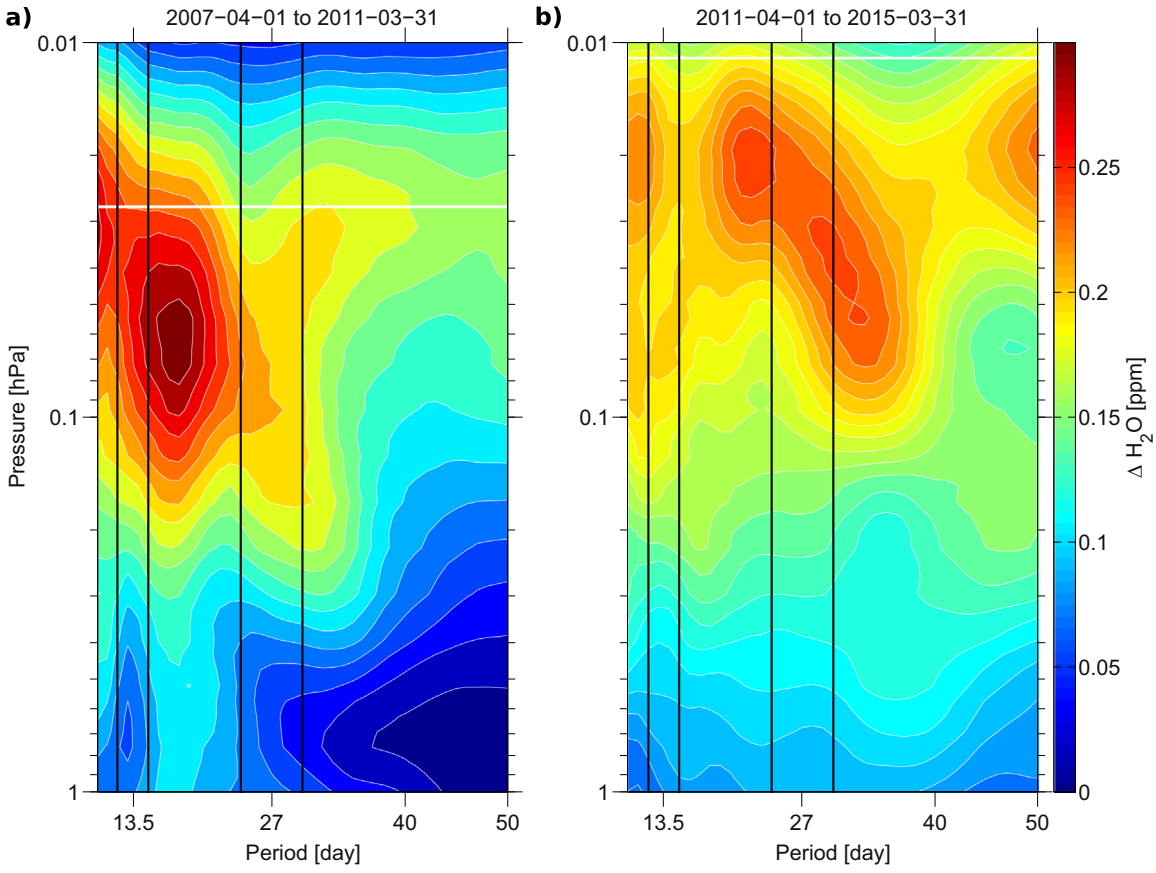

Fig. 4. Mean amplitude spectra of the MIAWARA water vapor time series above Bern as a function of pressure level, averaged for the whole time intervals from 2007-04-01 to 2011-03-31 (a) and 2011-04-01 to 2015-03-31 (b). The vertical black line pairs indicate the 27-day band and its harmonic at 13.5-day period. The horizontal white lines each show the mean upper measurement limit.

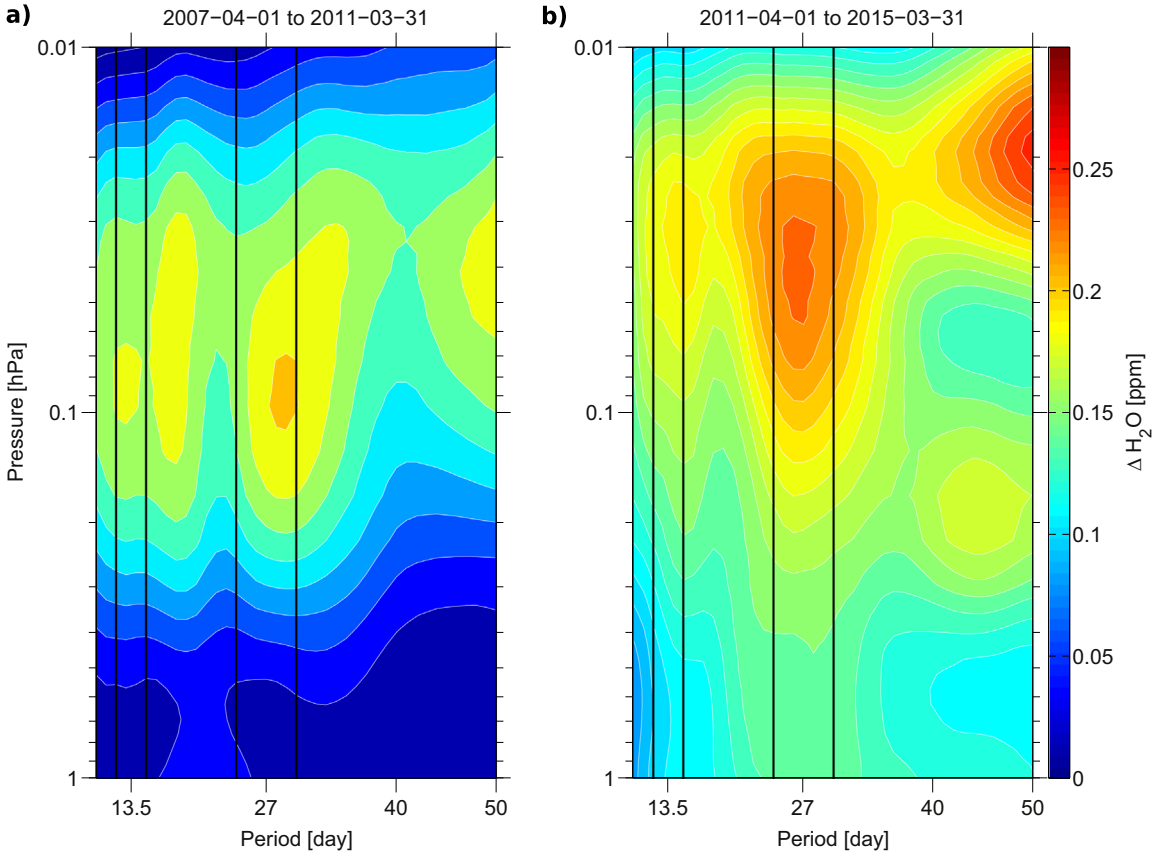

Fig. 5. Same as Fig. 4, but data are taken from Aura MLS satellite observation. The measurement coincident criterion is 400 × 800 km (meridional/zonal) from the location of MIAWARA. The MLS water vapor time series is convolved with the averaging kernels of MIAWARA, which has the lower vertical resolution.

was previously presented in Studer et al. (2012) and quite recently used to study the quasi 16-day wave in mesospheric H_2O (Scheiben et al., 2014). The filter suppresses oscillations with frequencies higher or shorter than the cut-off frequencies $f_c = f_p \pm 0.1{*}f_p$ around a central frequency $f_p = 1/T_p = 1/27$ d. The Hamming window has a size which is the triple-fold of T_p (central period), in order to ensure a fast response of the filter to the temporal data variability. The filter itself runs forward and backward along the geophysical time series with zero-phase lag, as recommended by Oppenheim et al. (1989).

Within this study, we define mean amplitude spectra (cf. Figs. 4 and 5) as average wave amplitudes from a spectral band-pass analysis of a data time series depending on the oscillation period. H_2O amplitude spectra are calculated by consecutively deriving the H_2O amplitude series at distinct periods from 10 to 50 days with a step of 1 day. The mean amplitude is obtained by averaging amplitude series over time. A final H_2O amplitude spectrum is created by plotting the time-averaged amplitudes as a function of the period. On the other hand time dependent relative H_2O wave amplitudes of the MIAWARA and Lyman-α 27-day oscillations are calculated, which help to analyze the temporal evolution of the 27-day signature in the time period from 2007-04-01 to 2015-03-31. The period of the Lyman-α oscillation is not restricted to exactly 27 days, but can range between almost 20 or reach above 30 days. Our cut off periods go from 24.3–29.7 days.

3.2. Estimating the power spectral density

Additionally to the mean H_2O amplitude spectra, derived according to Section 3.1, we analyze predominant oscillations in the MIAWARA data set with periods in the same range (10–50 days) by estimating the power spectral density (PSD) according to Welch (1967). Since the H_2O profiles of the microwave radiometer are retrieved on a constant pressure grid, the measurements on every pressure grid point are handled as an individual time series. These individual time series are divided into sections with length L of about 1 year (350 days). The default overlapping size is 50% of the section size and we apply a Hamming window function of the same size (350 days). With this method, the probability of the PSD estimate is obtained within a confidence interval of 95%.

The PSD is a statistical estimate and is in general a more detailed and accurate descriptor of the power content in a signal than taking the square of a FFT (Fast Fourier Transform). Let x_n label the nth segment of the H_2O signal x, N be the number, L the length of the data segments, i the index of the pressure level, U as given in Eq. (5), and FT_i the finite Fourier transforms, then the ith PSD estimate $P_x(i)$ is given by

$$P_x(i) = \frac{L}{UN} \sum_{n=0}^{N-1} |\mathrm{FT}_i(x_n)|^2 \tag{4}$$

The time dependent signal (amount of H_2O) is cut into overlapping segments (of length L) and an averaging of the squared-magnitude finite Fourier transforms FT is applied to a prior windowing of these signal sections with a Hamming window W_H

$$U = \frac{1}{L} \sum_{l=0}^{L-1} W_H^2(x_n) \tag{5}$$

At the end a time average of the individual periodograms is calculated to decrease the variance of the individual power spectra. The outcome is a vector of power measurements versus frequency or period bins. The windowing of sections is the typical step in the method of Welch to obtain a so called “modified periodogram”.

3.3. Cross-correlation analysis

Since our focus is on periodic oscillations with periods of approximately 27 days, we have deseasonalized the water vapor time series prior of calculating cross-correlations to solar Lyman-α. The H_2O data set has been processed with REMST, a MATLAB function that removes the trend and seasonal component by applying the moving average technique (Weron, 2007). In particular, the moving average-based annual component of the 365 day period was filtered out. Supplementary, the program eliminated a polynomial trend in the H_2O VMR (volume mixing ratio) time series.

Normalized cross-correlation coefficients between the water vapor time series and solar Lyman-α flux are calculated according to Bendat and Piersol (2000). The obtained coefficients indicate how sensitive mesospheric H_2O over Bern responds to the sun induced perturbations. The signal sequences are normalized with respect to the covariances at the zero phase lag.

Overall 121 lags from −60 to 60 days are considered in the cross-correlation analysis. We derive the statistical confidence on the 99% or 95% level for the computed correlation coefficients with the application of a hypothesis test that follows a Student's t-Distribution

$$t = \frac{r\cdot\sqrt{(N-2)}}{\sqrt{(1-r^2)}} \tag{6}$$

The Pearson correlation coefficient is given by r, the absolute number of compared data points to calculate r by N. By looking up a table of t-Distribution the confidence level of the correlation has been determined and will be used to identify areas of high and significant correlations between mesospheric H_2O and solar Lyman-α dependent on the pressure level and phase lag.

3.4. Wavelet analysis

With the band-pass filtering technique (Section 3.1) we analyze the temporal behavior of the 27-day oscillation amplitude and derive time averaged H_2O amplitudes in two 4 years periods. The temporal evolution of wave amplitudes for a larger range of periods could be obtained by applying band-pass filters with varying central periods to the data, but more sophisticated techniques, such as wavelet computations, are available.

A wavelet analysis is a powerful tool for investigating geophysical time series of for example ENSO (El Niño-Southern Oscillation) (Wang and Wang, 1996; Zhang et al., 2007), large scale atmospheric circulations like NAO (North Atlantic Oscillation) (Jevrejeva et al., 2005) or mesospheric planetary wave activity (Espy et al., 2005). A practical guide to the core of wavelet analysis is provided by Torrence and Compo (1998). They provide a direct comparison to the windowed Fourier transform. Further it is discussed how the choice of a wavelet basis function influences results, why edge effects due to the finite-length of time series are important, and how the wavelet scale is linked to the Fourier frequency. Most important, new hypothetical tests for the power spectra of the wavelets were developed by deriving theoretical wavelet spectra for white (random signals with a constant power spectral density) and red noise (signal noise produced by Brownian motion) processes with Monte Carlo simulations. Confidence intervals have been established in the code. This was an important step towards a more quantitative description of wavelet analysis results. In Section 4 we present plots, showing continuous wavelet transforms (CWT), cross wavelet transform (XWT) and wavelet coherence (WTC) of the data with the use of a software package developed by Grinsted et al. (2004), which is based on the preceding work of Torrence and Compo (1998).

We briefly summarize the mathematical ideas behind CWT, XWT and WTC in the following paragraphs. Overall, WTC and XWT are very useful to examine a suggested relationship between two data sets, in our case the MIAWARA H_2O and Lyman-α time series, in regard of the time-frequency space. In order to understand XWT/WTC we start to define the Morlet-Wavelet (Eq. (7)), the basic wavelet function used together with the wavelet software package.

$$\Psi_0(\tilde{t}) = \pi^{-\frac{1}{4}}\cdot\exp(\tilde{f}_0\tilde{t})\cdot\exp(-\tfrac{1}{2}\tilde{t}^2) \tag{7}$$

Here $\tilde{t}$ and $\tilde{f}_0$ characterize dimensionless time and frequency. The wavelet itself is kind of localized in time-frequency space. Alike for the cross-correlation analysis the H_2O VMR time series of MIAWARA is deseasonalized in a first step. Then a pressure layer averaging of the mixing ratios is performed, according to the different upper measurement limits for the two 4 year periods. For the first period (2007-04-01 to 2011-03-31) we use the pressure layer between 0.027 and 0.1 hPa, while for the second period (2011-04-01 to 2015-03-31) we use the layer between 0.011 and 0.1 hPa. For each reference period A and B, the Morlet wavelet is applied to the pressure layer averaged water vapor time series and Lyman-α data set as a band-pass filter. The result is a continuous wavelet transform (CWT).

The signal power of the CWT $W_n^X(s)$ (cf. Eq. (2) in Grinsted et al. (2004)) is given by $|W_n^X(s)|^2$. Edge effects arise from the fact that the core wavelet is not entirely localized in time. It is common to show the Cone of Influence (COI), defined as an area where the power of the wavelet is reduced to the e^{-2}-fold of the edge value. The local phase quantity can be estimated from the complex part of the CWT and the statistical confidence, which is $1-\alpha$ (significance level), can be specified proportional to the null hypothesis through a stationary process, where a particular background power spectrum is embedded.

Having the background knowledge about the CWT, the XWT of two different time series, in our case H_2O (X) and solar Lyman-α (Y), can be expressed as $W^{XY} = W^X W^{Y*}$. Y^* is the complex conjugate of Y. The absolute power of the XWT is computed with $|W^{XY}|$. It is possible to get information about the phase relationship of the data by looking at the complex argument of the cross wavelet transform. We note that in the XWT plot areas are visible where (in time-frequency space) our used data sets have high common power. Unfortunately this is not equivalent to a measure of correlation. Therefore the so called wavelet coherence (WTC) is introduced (see e.g., Torrence and Compo, 1998), which can be regarded as a localized and frequency dependent cross-correlation coefficient (values between 0 and 1). It is defined as the normalized square of the XWT power spectrum. The process of normalization uses the power spectra of the single pressure layer averaged H_2O and Lyman-α time series.

4. Analysis of the results

First of all the motivation and concept of the analysis is concisely presented to better understand the sequential presentation of our results. The idea of a possible solar–terrestrial relationship came up as we discovered increased variations in the retrieved amount of H_2O from the ground-based radiometer MIAWARA in the 27-day oscillation band after March 2011. Lyman-α irradiance data has been acquired and a band-pass filter with a central period of 27 days applied to the data sets. The temporal evolution of the amplitudes can give a first hint of a relation if the occurrence is simultaneous. As next logical step cross-correlations between the relative wave amplitude time series have been calculated for different altitudes. A more direct correlation is obtained with the real data series (not band-pass filtered) to identify the sign and

strength of correlation at different mesospheric pressure levels. A focus is set to a time during and after a solar superstorm event (2012-07-01 to 2013-01-31), where a separate cross-correlation analysis is performed. Since the wavelet analysis is a common tool in studying geophysical time series we had a closer look at it and processed the used date sets (Section 2) with an available software package, provided by Grinsted et al. (2004). The advantage here is that two time series can be analyzed with respect to common signal power in different periods and a localized (in time) correlation coefficient can be easily obtained. The data analysis in general splits up into two time periods, each four years long, where the variability of the Lyman-α irradiance on the 27-day scale is on average much weaker (reference period A: 2007-04-01 to 2011-03-13) than in the other time period (reference period B:

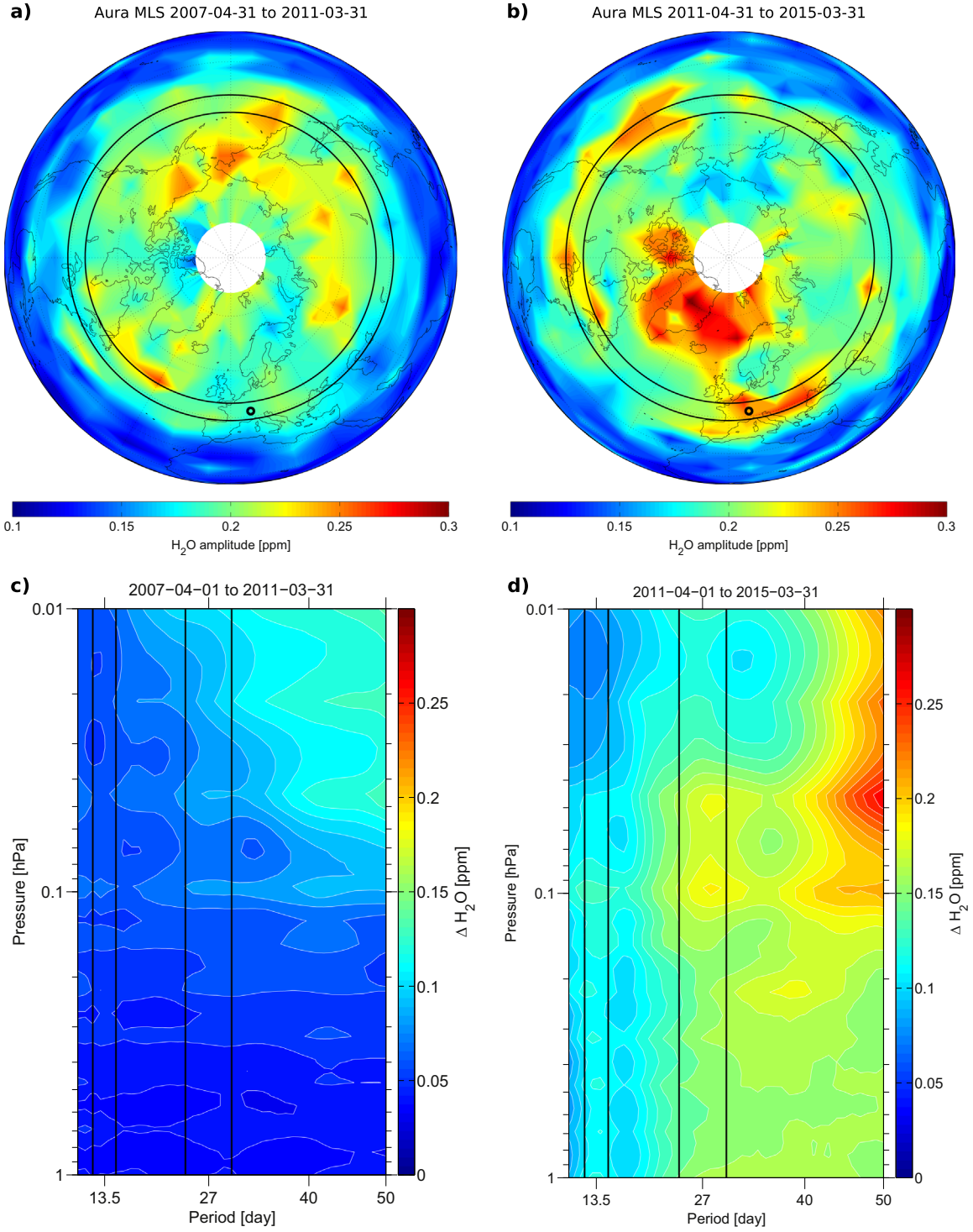

Fig. 6. *Upper panels*: Northern hemispheric distribution of the 27-day wave amplitude of water vapor at 0.04 hPa as derived from Aura MLS observations between 2007-04-01 and 2011-03-31 (a), respectively 2011-04-01 and 2015-03-31 (b). The black circle marks the location of the MIAWARA instrument, while the zonal black lines enclose the area for zonal mean satellite measurements used for the panels below. *Lower panels*: Mean amplitude spectra of Aura MLS zonal mean (44–50°N) water vapor time series as a function of pressure level, averaged for the time periods 2007-04-01 to 2011-03-31 (c) and 2011-04-01 to 2015-03-31 (d). The vertical black line pairs indicate the 27-day band and its harmonic at 13.5-day period.

2011-04-01 to 2015-03-13). Currently the sun passes trough solar cycle 24 which began on 4 January 2008. The general sunspot activity was minimal until the beginning of year 2010, what is affirmed by weak Lyman-α fluctuations (see Fig. 3). The variability of the solar Lyman-α amplitude can be seen in Fig. 3 and in addition in Figs. 9 and 14 together with different illustrations of the water vapor data. On the one hand the whole altitude dependent H_2O VMR time series is plotted, on the other hand pressure layer averaged H_2O series are shown.

From the local water vapor time series above Bern (Fig. 3) mean amplitude spectra in units of absolute H_2O VMR oscillation (Fig. 4) for two periods of equal length are derived in a first step according to Section 3.1. The two periods denote low (Fig. 4a) and high (Fig. 4b) Lyman-α oscillations within the duration of solar cycle 24. In Fig. 4a, a dominant 16-day oscillation with mean maximal amplitude of about 0.3 ppm is present between 0.05 and 0.08 hPa. The transition to the 27-day band region is smooth with decreasing amplitudes of H_2O oscillations. Fig. 4b is different, the highest amplitudes are within or close to the 27-day period band in the upper mesosphere. A 10 and 20-day modulation at 0.02 hPa is distinct and another wave amplitude maximum at 30 days (0.04 hPa). Regarding the time period B, the H_2O wave oscillations do not exceed 0.25 ppm.

We intercompare the mean amplitude spectra obtained from MIAWARA with those calculated from convolved MLS measurements within 400×800 km from Bern. The convolution is done with the averaging kernels from MIAWARA, the instrument with the lower vertical resolution. Fig. 5 shows the MLS amplitude spectra, the bases of the comparison to the MIAWARA results. It is apparent that in reference period B the agreement to MIAWARA is better than in period A. We point out, that this feature is not related to any specific high biases to Aura MLS observations as we can conclude with the outline of Section 2.1. The position and strength of the wave patterns matches quite well, although small differences are visible. For instance, the MLS spectra in Fig. 5b have an explicit maximum in the center of the 27-day band, whereas the MIAWARA counterpart spectra are not clearly locked to the center of the band. The spectra for periods above 24 days in reference period A show similar patterns in the MLS and MIAWARA plot (amplitudes up to ~0.2 ppm), but the absolute amplitudes for the 16-day wave pattern are higher by more than 0.1 ppm in the MIAWARA data (Fig. 4a). For both MIAWARA and MLS derived results the fact of enhanced wave amplitudes of the 27-day oscillation in reference period B compared to A is valid.

At this point we want to make use of global MLS data to show how the 27-day H_2O wave amplitude is distributed over the Northern Hemisphere and how zonal mean amplitude spectra according to Fig. 5 look like for the latitude belt between 44 and 50°N. Fig. 6 treats both time periods A and B separately as handled throughout the paper. The zonal mean amplitude spectra are derived as done for Fig. 5, with the difference that zonal mean water vapor measurements are used. The hemispheric distribution of the 27-day wave amplitude is shown at the 0.04 hPa pressure level for period A (Fig. 6a) and B (Fig. 6b). The 27-day wave amplitudes show structures in horizontal direction. Maxima over specific locations can be found for both studied periods. Larger areas of higher amplitudes exist for period B. We are aware of the fact that it is dependent on the measurement location if a difference in the mean 27-day amplitude is observed between the lower and higher solar activity period. Large parts of Europe, including the location of MIAWARA, show these different behaviors. The zonal mean spectral analysis reveals that local maxima in the period spectrum show up in the 27-day and also but less distinct in the 13.5 day band (Fig. 6d). For the 27-day band the H_2O amplitudes are largest (up to 0.2 ppm) in the pressure range 0.1 – 0.04 hPa. Compared to Fig. 6c and the same period and pressure regime, the H_2O amplitudes reach less than half of the value (<0.1 ppm) during period B.

In order to get information about the confidence and to check for consistency, a second method (Section 3.2; PSD estimate) to

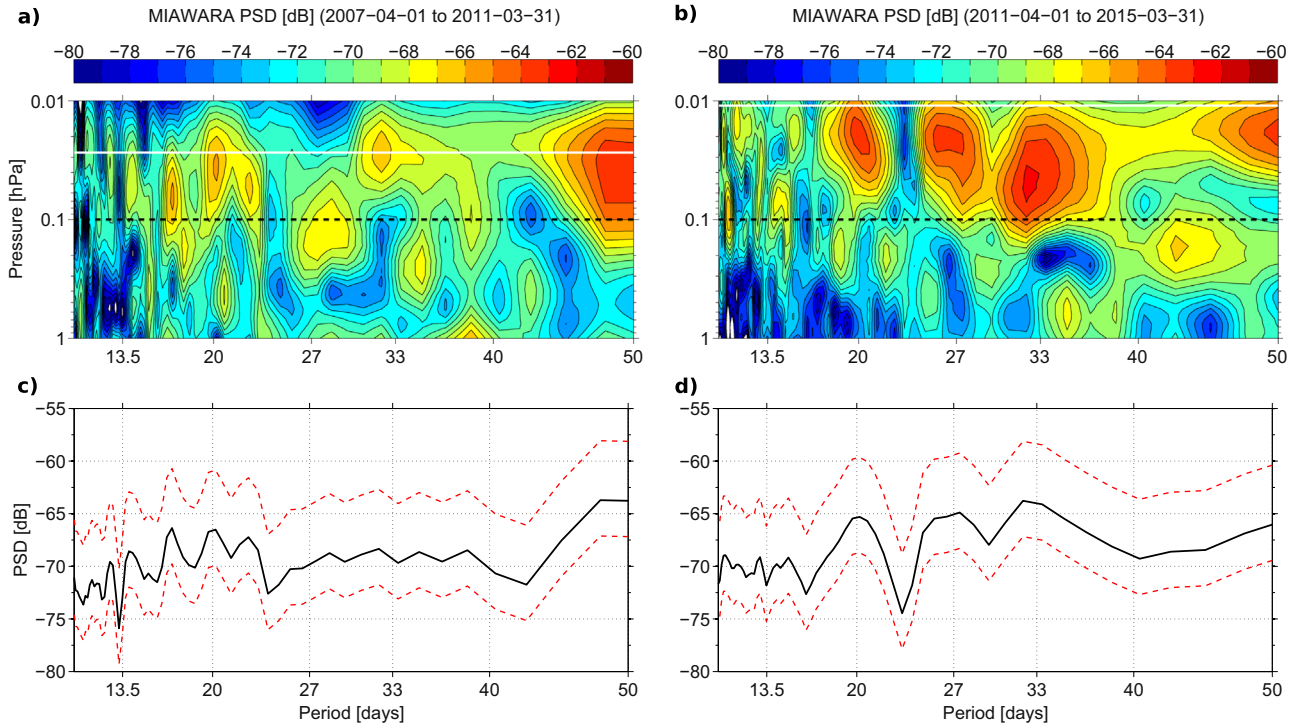

Fig. 7. MIAWARA periodogram from water vapor time series (a, c): 2007-04-01 to 2011-03-31; (b, d): 2011-04-01 to 2015-03-31 showing the Power Spectral Density (PSD) in a oscillation period range from 10 to 50 days. Top panels: PSD contour plots between 1 and 0.01 hPa. Bottom panels: Mean PSD line plots (black) with 95% confidence intervals (red dashed lines) between 0.1 and 0.027 hPa (left) and 0.1 and 0.011 hPa (right). The lower limit of 0.1 hPa is indicated in the contour plots by horizontal black dashed lines and the upper limit by the white lines. (For interpretation of the references to color in this figure caption, the reader is referred to the web version of this paper.)

calculate a MIAWARA water vapor periodogram has been applied.

In the contour plots of Fig. 7a and b the power spectral density is given in units of decibel. Patterns of the 16-day and 20-day wave show similar high PSD values (~ – 66 dB) in reference period A, right below the mean upper measurement limit of 0.027 hPa. The 20-day signal peaks out stronger with around –63 dB in reference period B (Fig. 7b). It appears that at higher periods some signals are at least as pronounced as the signal power around 20 days. Although there are high contributions in the power spectrum beyond 30-day periods, increasing at 32–33 days (cf. Fig. 7a and b) and beyond 45 days, we center our focus to periodic variations of mesospheric H_2O within the range of 24–30 days (27-day band). The periodogram on the right side of Fig. 7 mark relative high PSD values at periods 27–30 days. The 27-day wave activity between April 2011 to March 2015 is higher by 5 dB compared to the years before, as the focus on the difference between the contour plots reveals.

Photochemical interactions between the radiation from the sun and water vapor are more likely to be detectable in the upper mesosphere. Thus the attention is put to the uppermost sensitive pressure layers above 0.1 hPa to the upper measurement limit that is derived from a measurement response criterion (>0.6) in the H_2O retrievals. Due to instrumental upgrades, the pressure layer for reference period B is 0.016 hPa thicker (roughly 6.2 km) than that of A. Fig. 7c and d show the mean power spectral density for the 0.1–0.027 hPa, respectively 0.1–0.011 hPa pressure layer with 95% confidence intervals. Investigating periods from 24 to 30 days, it is realized that the magnitude of the PSD shows a peak in reference period B (7d) and by contrast only a slight increase at a low PSD level in Fig. 7c. We note that the maximum of the 20-day wave has a similar high PSD (~ – 65 dB) as the adjacent maximum of the 27-day oscillation.

As any common 27-day features are hard to see by comparing the plots in Fig. 3, a plot of the time dependent relative wave amplitude is presented in Fig. 8a. Starting with the beginning of 2011 the relative wave amplitudes of the solar signal start to intensify with an irregular sequence of high and low relative amplitudes. About 10% are reached in November 2012, respectively 15% in July 2014. The absolute maximum in July is preceded by a relatively high and constant amplitude of more than 5% since the third quarter of year 2013. Wave activities up to 15% in relative H_2O magnitude are accompanying this event in the upper

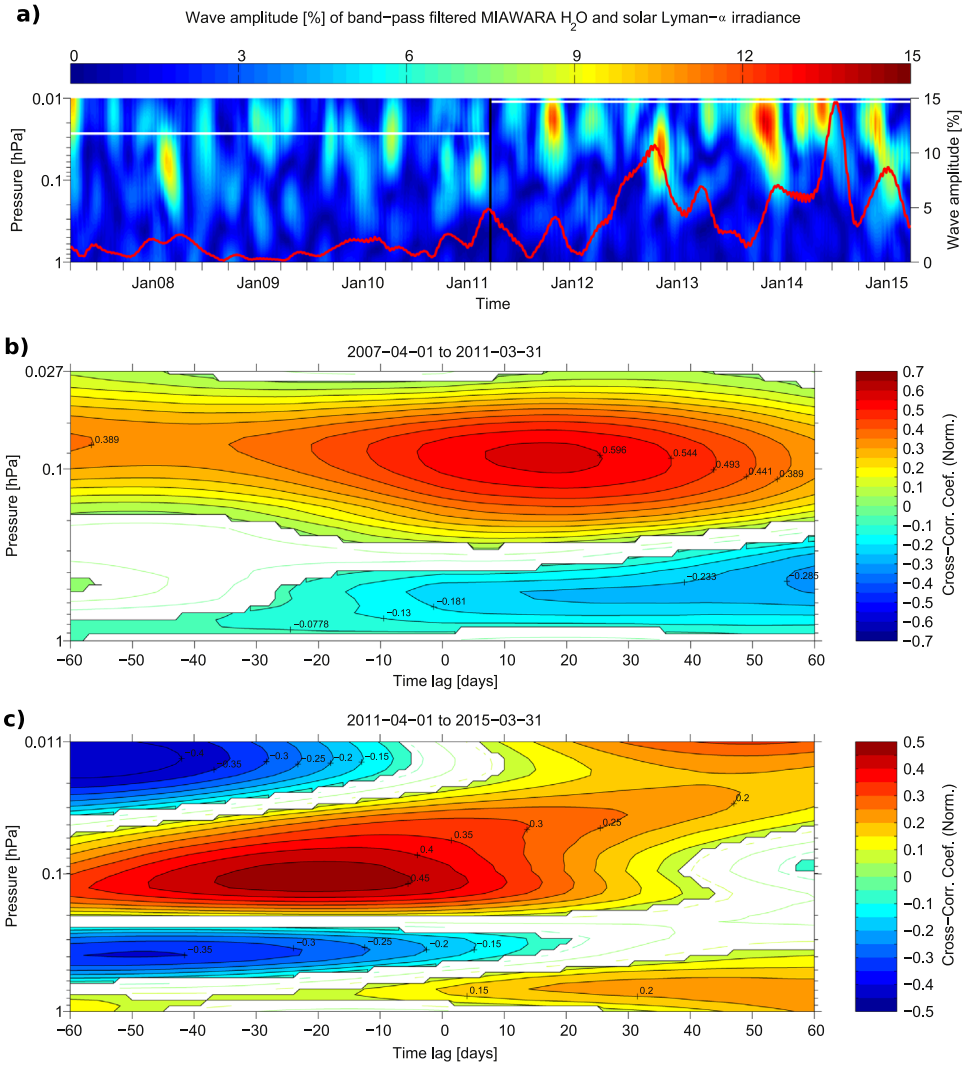

Fig. 8. (a) Relative wave amplitudes of the band-pass filtered time series of water vapor as observed by MIAWARA (contour plot) and solar Lyman-α composite (overlapped red line plot). The limits of the lower and upper band-pass windows are $\pm$ 10% of the central period of 27 days. Please consult the text for details about the calculation method. The horizontal white lines indicate the upper mean measurement limit of MIAWARA. (b) Cross-correlation between band-pass filtered data time series in the pressure range 1 – 0.027 hPa and time period 2007-04-01 to 2011-03-31. The filled contours show the height dependent normalized cross-correlation coefficient with statistical confidence ≥99%. Lower confidence levels are shown by unfilled contours. (c) Same as (b), except for time period 2011-04-01 to 2015-03-31 and pressure range from1 – 0.011 hPa. (For interpretation of the references to color in this figure caption, the reader is referred to the web version of this paper.)

mesosphere. These results lie within regions of sufficiently high measurement responses of the ground-based instrument. Other time frames where the MIAWARA H_2O and solar Lyman-α 27-day band-pass amplitude signatures coincide well are March 2008, November 2012 and January 2015. Further we can record that the H_2O band-pass analysis between April 2007 and March 2011 (weak relative wave amplitudes in solar Lyman-α) shows also weaker relative amplitudes for 27-day oscillations like during times of higher solar Lyman-α activity (reference period B).

The strongest observed amplitudes in water vapor are present above 0.1 hPa. High positive correlations are present near 0.1 hPa (Fig. 8b and c). The highest positive normalized cross-correlation coefficients reach values of about 0.6 and 0.5 with time lags of around 20 days between the water vapor and solar Lyman-α band-pass signal. A major difference of the two reference periods is the sign of the time lag where the maximum occurs. In Fig. 8b (period A) the time lag is positive (Lyman-α wave amplitude signal leading by 10– 20 days), whereas in Fig. 8c (period B) it is negative (H_2O wave amplitude signal leading by 10–30 days). The negative value of the lag can be explained with the photodissociation lifetime (>10 days) of H_2O at these altitudes and latitudes (McCormack et al., 2008).

A similar analysis to the prior shown band-pass signal correlation (Section 3.3) to detect direct correlations has been motivated and included. The cross-correlation plot between the investigated data time series shows the average correlation considering the common reference periods. By inspecting the color plot in Fig. 9b and d it is confirmed that MIAWARA H_2O data time series are negative correlated (confidence level ≥99%) to the irradiance flux of the sun at Lyman-α wavelength in the pressure region of interest (above 0.1 hPa).

The strongest normalized cross-correlations, with coefficient values of −0.45 (Fig. 9b) and −0.3 (Fig. 9d), are located near the 0.04 hPa pressure level which is equivalent to an altitude of approximately 70 km. The occurrence of the main correlation minima in the time lag space reveals a relative phase lag of 6–10 days for both periods.

Side lobe minima occur at time lag shiftings close to $n \times 27$ days, with $n \in \mathbb{Z}$. Below 0.2 hPa the confidence level cannot be maintained in reference period A and gaps in the pressure versus time lag contour plot (filled areas) show up. For the second studied period it is different. Correlation coefficients of approx. −0.25 to −0.3 within the 99% confidence level can be found below 0.2 hPa and with time lags between 40 and 60 days. In Section 5 the attention is put on a time period (July 2012 to February 2013), where magnetic energy of the sun (stored in magnetic flux tubes), was released in several events (solar flares). Fig. 9c shows very high and pronounced Lyman-α oscillations during that time. Next we complete the section, showing findings from wavelet computations (Section 3.4), as it is easy to illustrate, how localized variations of water vapor and Lyman-α look like in time-frequency space.

The wavelet transform plots in Figs. 10 and 11 provide an overall view of occurring period modes in the two time series. The main advantage to the previous presented PSD or mean amplitude spectra analysis is that we can now look at temporal wave features in middle atmospheric H_2O and are not restricted to a picture of a time average. In return of gaining the time dimension, the altitude information is lost in a single plot. For the whole wavelet study (CWT, XWT, WTC) we choose pressure layer averaged (0.1–0.027 hPa for reference period A; 0.1–0.011 hPa for reference period B) ground-based H_2O VMR observations that are deseasonalized. The processed data time series are shown in Fig. 9a and c.

We state that on the 95% confidence level, the highest wavelet power (~16 in units of normalized variance) in the MIAWARA data is observed at periods of 16–20 days between April 2007 and March 2011 and in addition but less frequent in the 27-day band (marked by the horizontal black lines; s. Fig. 10a). Moving over to

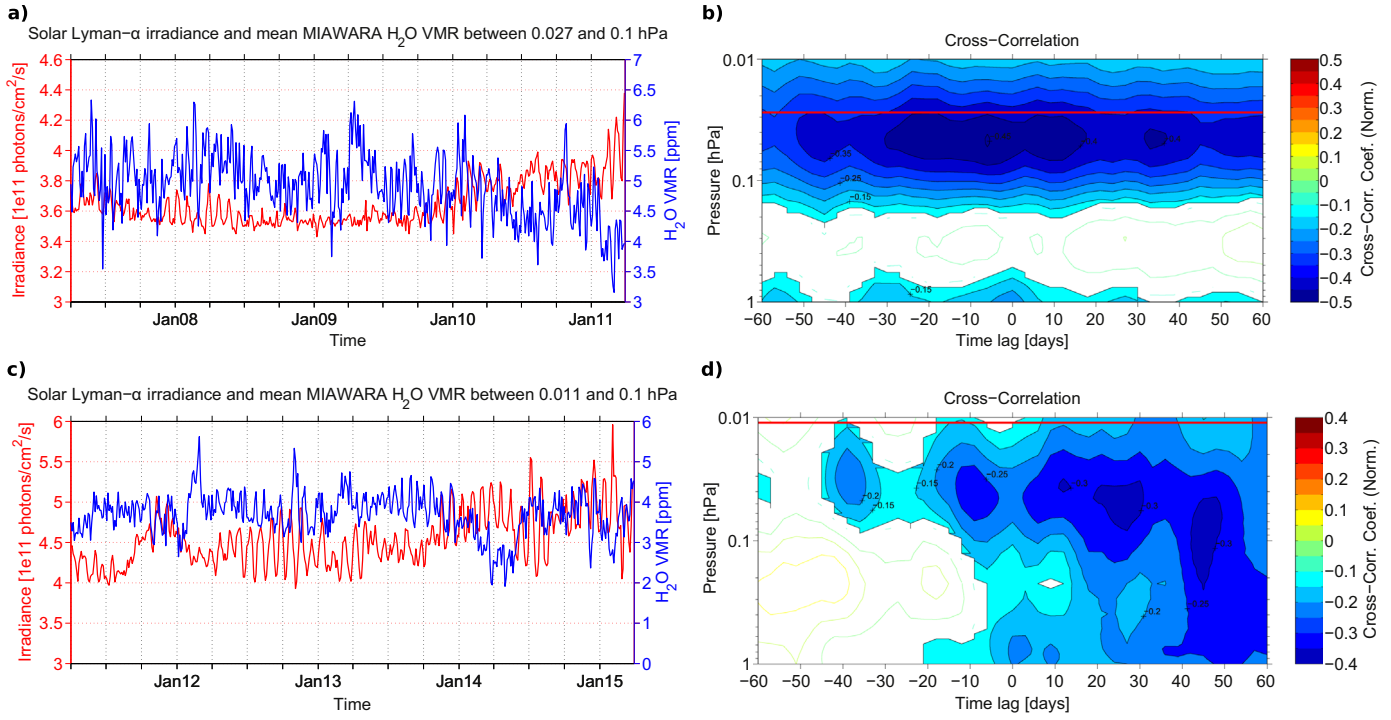

Fig. 9. Pressure layer averaged (0.027–0.1 hPa, 0.011–0.1 hPa) and for deseasonalization filtered MIAWARA water vapor time series (blue line) and irradiance of solar Lyman-α composite (red line) is plotted in (a, c). While cross-correlations between composite solar Lyman-α irradiance and MIAWARA water vapor time series in the pressure range 0.01 – 1 hPa are shown in (b, d). The filled contour plots show the height dependent normalized cross-correlation coefficient with statistical confidence ≥99%. Lower confidence levels are shown by unfilled contours. The horizontal red lines indicate the upper mean measurement limit of MIAWARA in the corresponding time period. (For interpretation of the references to color in this figure caption, the reader is referred to the web version of this paper.)

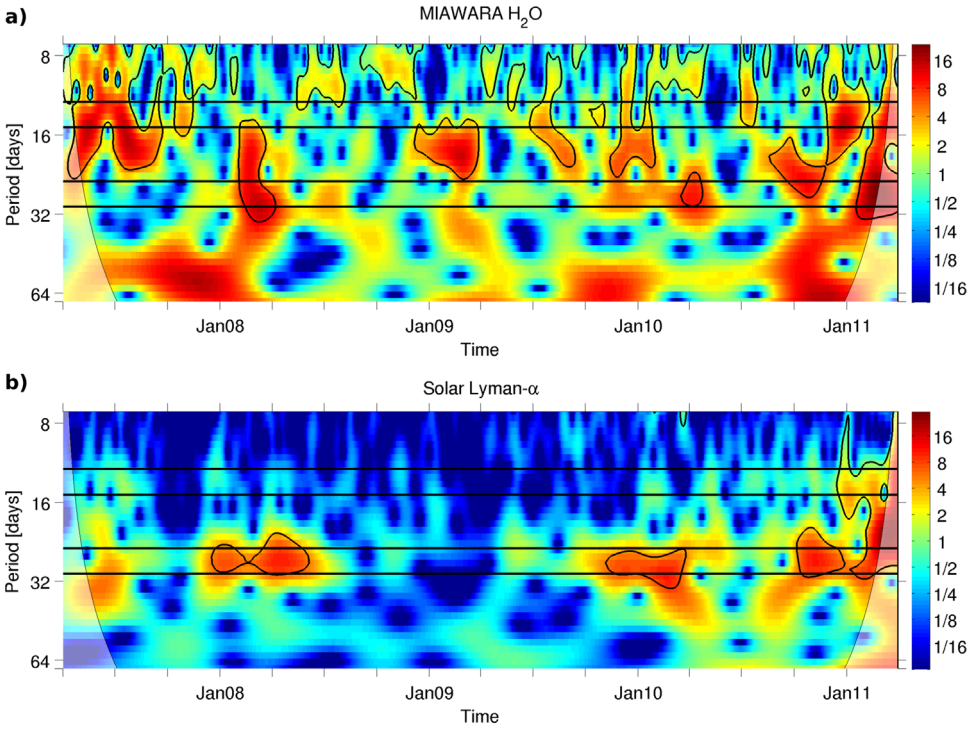

Fig. 10. Continuous wavelet transform (CWT) of mean (0.1–0.027 hPa) deseasonalized MIAWARA H_2O VMR (a) and solar Lyman-α composite (b), showing the wavelet power in units of normalized variance in the period of low solar Lyman-α oscillations (2007-04-01 to 2011-03-31). The 95% confidence level against red noise is shown by the black contours and the cone of influence (COI), where edge effects probably misrepresent the analysis, is separated by a lighter shade. The 27-day and its harmonic band (13.5-day) are indicated by the horizontal black line pairs. (For interpretation of the references to color in this figure caption, the reader is referred to the web version of this paper.)

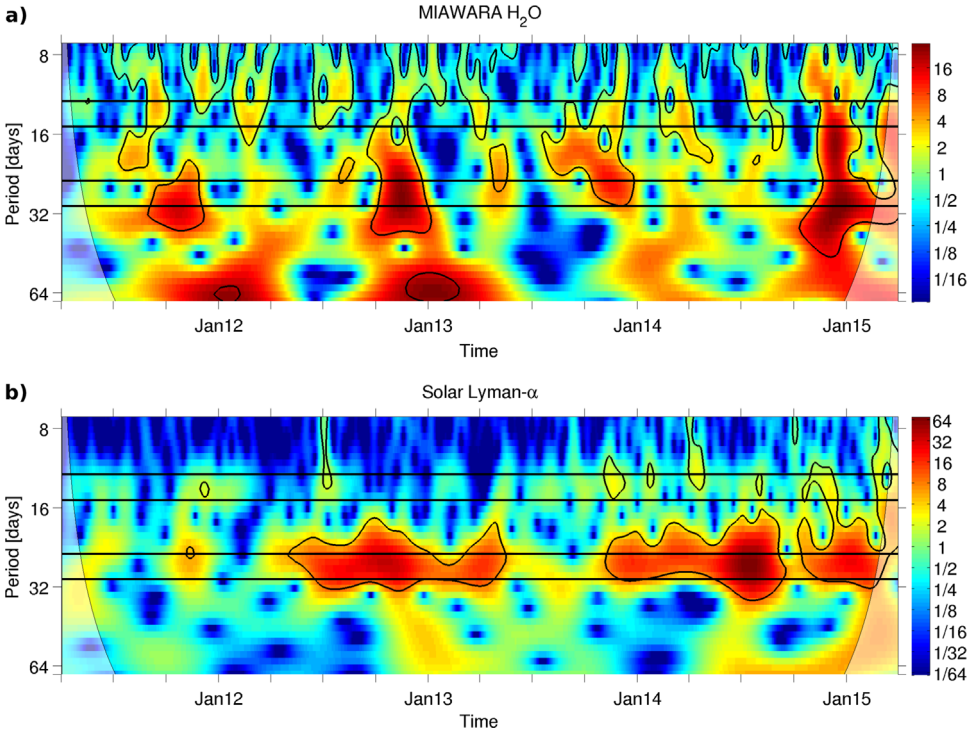

Fig. 11. Same as Fig. 10, but for the time period from 2011-04-01 to 2015-03-31.

period B more often high wavelet power comes from 27-day oscillations (Fig. 11a). It is therefore worthwhile to measure common signatures between MIAWARA H_2O and solar Lyman-α in time quantitatively. This is achieved by the cross wavelet transform (XWT, Figs. 12a and 13a) and wavelet coherence (WTC, Figs. 12b and 13b) analysis.

With the beginning of January 2011 the sunspot activity of solar cycle 24 is intensifying as it can be seen with the CWT power of the Lyman-α (cf. Figs. 10b and 11b). During the enhanced solar activity at Lyman-α wavelength the XWT investigation shows that

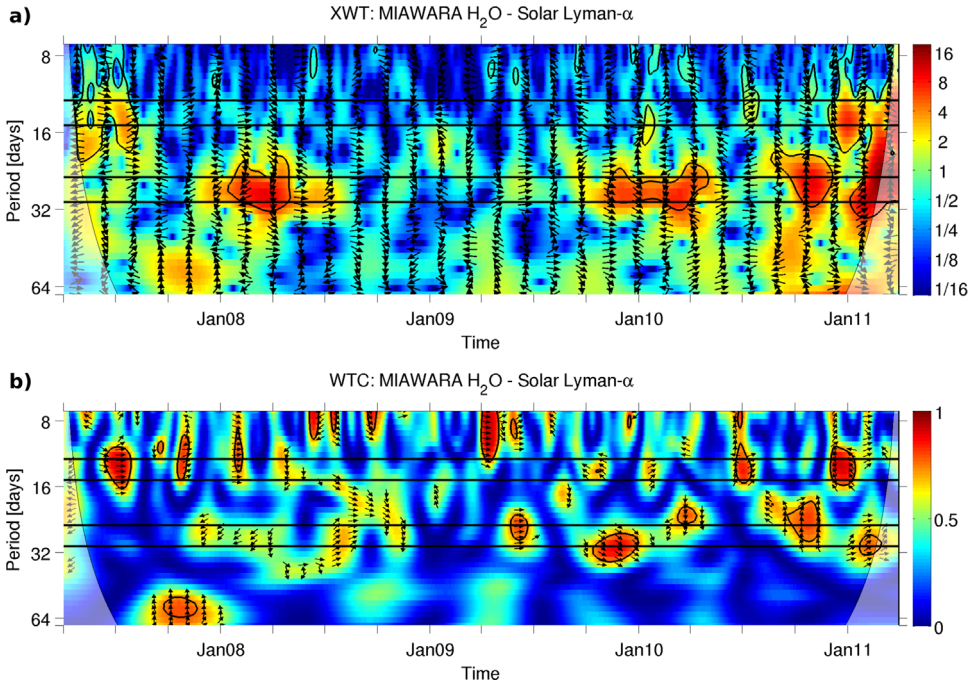

Fig. 12. Power of cross wavelet transform (XWT, (a)) between mean MIAWARA H_2O VMR (0.1 – 0.011 hPa) and solar Lyman-α irradiance composite in units of normalized variance and squared wavelet coherence (WTC, (b)) of the two time series is plotted in the period of low solar Lyman-α oscillations (2007-04-01 to 2011-03-31). The 95% confidence level against red noise is shown by the black contours and the cone of influence (COI), where edge effects probably misrepresent the analysis, is separated by a lighter shade. Black arrows illustrate the relative phase relationship between MIAWARA H_2O and solar Lyman-α (*Pointing right*: In-phase. *Pointing left*: Anti-phase. *Pointing straight down*: MIAWARA H_2O leading Lyman-α by 90°). The 27-day and its harmonic band (13.5-day) are indicated by the horizontal black line pairs.

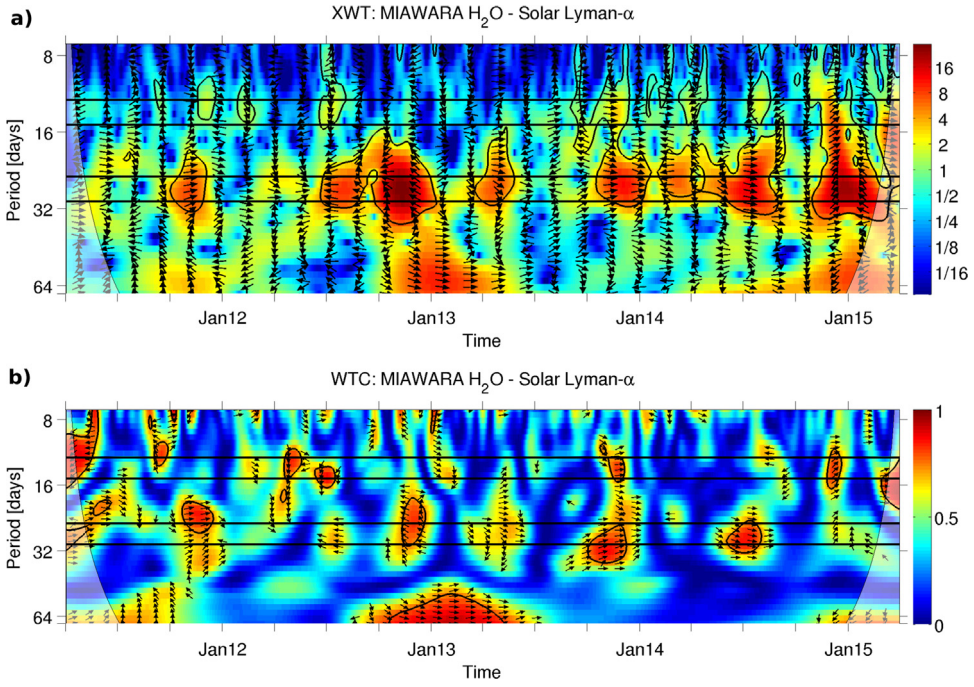

Fig. 13. Same as Fig. 12, but for the time period from 2011-04-01 to 2015-03-31.

the two signals have significant common power in the solar induced period bands. This is valid for the 27-day and the 13.5-day band whereby the latter has reduced common power on average. High common power on the two month cycle around January 2013 (Fig. 13a) cannot maintain a confidence of ≥95% against the simulated red noise.

The direction of the arrows in the vector field indicate the phase relationship. We find some of the signatures with significant high common wavelet power to be in-phase (rightward pointing arrowheads). In particular the time window between November 2013 and January 2015, where the relative wave amplitude of the solar irradiance has a major maximum (Fig. 8a), shows in-phase behavior. Nevertheless, a clear phase lock cannot be assigned to the time series as long as anti-phase sectors, for instance between July 2012 and January 2013, are present (Fig. 13a). Implications out of this are addressed during the discussions (Section 6). A measurement of high common power does not automatically imply a high correlation. In order to see whether there are coherent

sectors, confirmed by statistical confidence, in the time frequency space of the XWT, diagrams of the squared wavelet coherence (WTC, s. Section 3.4) are added in Figs. 12b and 13b.

Regarding the WTC, it is useful to think of a correlation coefficient that appears in the time-frequency domain. Significant correlations between the pressure layer averaged H_2O measurements above Bern and solar Lyman-α irradiance on the 27-day period scale arise intermittently (coefficients up to 0.8–0.9), albeit preferentially during time sections where the cross-wavelet transform plots show high common power. In general the in-phase behavior can be found more often in the black marked solar period bands (Figs. 12b and 13b). On a two month period scale, correlation coefficients above 0.8 appear during October 2012 to May 2013. Grinsted et al. (2004) declares that time-frequency domains in a WTC plot with a confidence level below 95% do not indicate an adequate causality. Therefore we confined the analysis to areas in the contour plots (inside of the black edging), where this criterion is fulfilled.

5. Correlation after the July 2012 solar superstorm

In this section we investigate the cross-correlation coefficient in detail for a short time period between July 2012 and February 2013. An extreme solar superstorm event in July 2012 introduced this interesting period, where the solar Lyman-α irradiance oscillations were particularly strong. Liu et al. (2014) reported about this severe space weather event, which would have had a comparable negative Disturbance Storm Time (DST) index as the pre-space age 1859 Carrington event (Carrington, 1859). Fortunately, two consecutively released coronal mass ejections (CMEs) on July 23, 2012 missed Earth.

Fig. 14a shows a prominent anti-correlation between the red and blue lines from July to mid-September 2012 and from November to January 2013. Absolute irradiance fluctuations on the 27-day scale regularly exceed 5×10 photons cm^{-2} s^{-1}. With a statistical confidence of ≥95% the highest correlations (see Fig. 14b), respectively anti-correlations, occur close to the 0.1 hPa pressure layer and reach values of almost −0.3 (zero time lag) and 0.4 (~13.5 days ahead). The solution with the higher lag value is physically more reasonable because it is associated with a time delay of the H_2O response (due to photochemical lifetime). The difference in the lag solutions is due to the shift of the solar Lyman-alpha time series. It indicates half of the 27-day cycle time scale. Still it has to be considered that a solar superstorm event is investigated and under such conditions a zero time lag solution could be due to the disturbed energetics, dynamics and photochemistry of the MLT region.

6. Discussions

Within this study the focus was primarily on the 27-day oscillation of mesospheric H_2O as observed above Bern (mid-latitudes, 46.88°N) by ground-based microwave radiometry. We tried to relate the observed quantities in the mean wave amplitude spectra (Figs. 4 and 7) to oscillations in the Lyman-α irradiance of the sun. Different data analysis methods (PSD, band-pass, cross-correlation, wavelet), and comparisons to satellite observations, have been applied. Cross-correlations were explored either on the 99 (Fig. 9) or 95% (Fig. 14) confidence level, as example.

Regarding the current solar cycle 24 (since January 2008), it is in general agreement that the sunspot activity was by far not as extreme as in Cycle 23 (May 1996 until January 2008) or Cycle 22 (September 1986 until May 1996). While Cycle 22 (23) produced a maximal sunspot number of roughly ~156 (~121), Cycle 24 was much more quiet with maximal ~82 sunspots recorded in April 2014. It presumably is the solar cycle with the lowest registered sunspot activity since 1750, when precise records began. Under these conditions it is likely more difficult to identify sun signatures in the H_2O data set within the studied time period (April 2007–March 2015). Still, the comparison of the power spectral density (PSD) in Fig. 7a and b between the solar low and high activity reference periods A and B, shows enhanced wave activity in proximity of the 27-day band above 0.1 hPa (64 km altitude). A second analysis of mean amplitude spectrum, derived from consecutive applied band-pass filters at different periods, supports the finding of the PSD analysis.

We emphasize that the present study is to our knowledge the first ground-based observation of the response of middle atmospheric water vapor to the 27-day solar rotation cycle, and our ground-based observations generally confirm the results obtained by the satellite experiment Aura MLS at mid-latitudes. Discrepancies occur for a range of periods around 16–20 days during the low solar activity period (A). There MIAWARA H_2O amplitudes are higher by 0.1–0.15 ppm (centered between 0.1 and 0.03 hPa). However, the monthly mean relative differences (see Fig. 1) do not show any abnormality in this pressure range and stay below ~5%. A conceivable explanation could be, that limb observations of satellites (e.g. Aura MLS) tend to smooth out existing atmospheric structures due to horizontal inhomogeneity. A ground-based instrument, such as MIAWARA, measures radiation in a narrow beam of approximate 5° and retrieves profiles that belong to a narrow geographical location.

A comparison between Fig. 6a and b reveals that the NH distribution of the 27-day wave amplitude as derived from MLS has a difference between tropical and subtropical regions that is by far smaller than for the polar or mid-latitude regions. One could

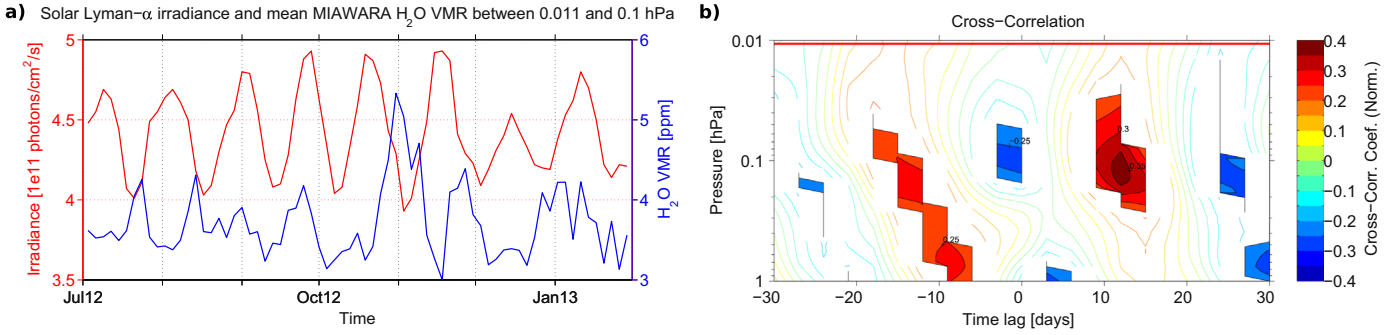

Fig. 14. Pressure layer averaged (0.011 – 0.1 hPa) and for deseasonalization filtered MIAWARA water vapor time series (blue line) and irradiance of solar Lyman-α composite (red line) between July 2012 and February 2013 is plotted in (a). While cross-correlations between composite solar Lyman-α irradiance and MIAWARA water vapor time series in the pressure range 0.01 – 1 hPa are shown in (b). The filled contour plots show the height dependent normalized cross-correlation coefficient with statistical confidence ≥95%. Lower confidence levels are illustrated by unfilled contours. The horizontal red line indicates the upper mean measurement limit of MIAWARA for the corresponding time period. (For interpretation of the references to color in this figure caption, the reader is referred to the web version of this paper.)

speculate that this feature is supporting more the dynamical planetary wave triggering theory by solar Lyman-α oscillations (at least for the higher latitudes) than a direct observation of photodissociation mechanism.

Moving over to a short discussion of the band-pass analysis, it is difficult to estimate whether prominent wave features are directly linked to the irradiance oscillations of the sun. Especially when the relative amplitudes do not exceed the magnitude of the expected errors, e.g. below 5% in case of Lyman-α. An example would be March 2008, where H_2O wave amplitudes exceed 10% while the wave amplitude triggered by Lyman-α is still below 5% (Fig. 8a, red line). With the height-dependent cross-correlation coefficients of the band-pass filtered data series we distinctly mark the altitude region where the highest coincidence is located (~0.1 hPa). The interpretation of Fig. 8b and c is difficult because the origin of the observed difference in the time lag is speculative. We note that positive coefficients at 0.1 hPa with a negative phase lag in reference period B support a link between the relative wave amplitudes (response leads forcing). During period A, where the opposite is apparently the case (forcing would lead response) it is clear that other processes than Lyman-α oscillations dominate the water vapor oscillations.

A 27-day variation due to a recurrent geomagnetic activity has been observed in mesospheric nighttime O_3 and OH (Fytterer et al., 2015). These and other possible influences, such as the occurrence of stratospheric warmings, on our results have to be considered. Mayr et al. (2009) suggested that monthly oscillations in stratospheric temperature fields play an important role in the background conditions associated with SSWs and that a physical correlation between a SSW and a measured 1–2 monthly variability of atmospheric parameters (e.g. temperature) exists. It is also possible that solar UV and Lyman-α perturbations trigger planetary waves with a 27-day mode, as the study by Krivolutsky et al. (2003) showed. Generally, a competition between periodic advection and periodic photodissociation loss of water vapor is present.

The pressure and time lag dependent cross-correlation coefficients have been studied for the whole defined reference periods separately (Fig. 9) and for a selected seven months period right after the July 2012 solar superstorm (Fig. 14). The absolute coefficient values (after Pearson) in the most interesting time periods are around 0.3. This is a medium to low correlation, dependent on the interpretation, and does not ensure a causal physical coherence by default. In our calculations detrended data was used to exclude seasonal variability. For future investigations it could be interesting to exclude also other factors like methane emission or gravity wave events and thereby expected outliers in the water vapor time series to increase the knowledge about the coupling processes, but this is beyond the scope of this paper.

The negative sign of the coefficients in the upper mesosphere for reference period B supports the view that effects of H_2O photodissociation by Lyman-α radiation and or planetary wave interactions (Krivolutsky et al., 2003) are observed. The phase lag between H_2O and solar variability in the Lyman-α band is centered between 6 and 10 days and this is in general agreement to the results in the paper of Shapiro et al. (2012), where 27-day oscillations in mean tropical H_2O (>78 km altitude) observed by Aura MLS revealed a phase lag in the order of 6–7 days. As one would expect, the negative correlation is found to be higher (~ -0.74), which is caused by the investigated tropical zone where the radiation flux from the sun is higher than at mid-latitudinal locations on the one hand and the used zonal mean satellite data on the other hand. The origin of the non-zero phase lag between mesospheric water vapor and solar Lyman-α is uncertain. While Shapiro et al. (2012) ascribes this feature to the long chemical lifetime of H_2O at high altitudes, an influence of a recurrent geomagnetic activity (Fytterer et al., 2015) is likewise conceivable.

The relatively low temporal resolution of the ground-based water vapor retrievals (3 days) was chosen to increase the signal to noise ratio. With this setup waves referred to the 2, 4 and 5-day scale were suppressed in the data set. The influence of possible interaction of waves with higher periods should be reduced. The lower period limit of our analyses has been set to 10 days accordingly.

Like with the time-lag dependent correlation results shown before, a sustaining phase lock has not been observed even with the cross wavelet transform or wavelet coherence analysis (Figs. 11 and 12). It is known that solar irradiance oscillations tend to shift their phase irregular and therefore shifting phase relations (time lags) could be expected. At least after the solar superstorm in 2012 (Section 5), when strong fluctuations of Lyman-α radiation were pronounced, an obvious anti-correlation of the H_2O and solar data time series has developed with nearly zero phase lag.

Simulations with the Met. Office coupled chemistry-climate model, performed by Williams et al. (2001), showed that the O_3 response to solar UV oscillations is likely to be significantly controlled by radiative induced dynamical effects in the middle atmosphere. Similar processes are considered for mesospheric water vapor by advanced numerical models. Especially photochemistry models designed for coupled radiative-chemical-dynamical modeling studies, like SOCRATES or HAMMONIA, could be of benefit and increase the understanding. Some model studies already demonstrated how the 11-year solar flux variability influences the photochemistry of ozone (Khosravi et al., 2002; Schmidt et al., 2006) and few (e.g. Gruzdev et al., 2009) modeled the impact of the solar rotational cycle on the upper atmosphere. Although in the paper of Gruzdev et al. (2009) the main chemical focus is on ozone, a short part is dedicated to water vapor. The model result showed, that a significant H_2O response in the extra-tropics is only present above ~75 km and it leads the solar forcing by around 8–11 days dependent on latitude and altitude, what is in good agreement to our results for reference period B. In general the responses (chemical and thermal) are seasonal dependent in mid and high latitudes and the response sensitivities are non-linear (drop-off with increased solar forcing). Compared to the thermosphere, thermal and chemical responses are more temporary in the stratosphere and mesosphere, despite the assumption of a constant solar forcing in the model. The results in Gruzdev et al. (2009) are in agreement with Ruzmaikin et al. (2014) (zonally averaged CO) and our findings in the band-pass and wavelet coherence analysis (mid-latitudinal H_2O).

7. Conclusions

In this study one of the first ground-based observation of a 27-day oscillation in mesospheric water vapor has been presented. We have shown that the observed wave amplitudes at the 27-day band in the upper mesospheric H_2O data above Bern can be related to the investigated solar irradiance variations of the Lyman-α (121.56 nm) spectral line. The observed relationship can be due to chemical (photolysis) as well as dynamical perturbations, induced by the solar variability.

The wave amplitudes showed a coherent behavior, most distinctly close to the 0.1 hPa pressure level. Substantial signs of frequent high correlations regarding the amplitudes of mesospheric H_2O and solar variations in the Lyman-α band were found. After 2011 high relative wave amplitudes occurred in temporal proximity to each other and altitude regions of highest coincidence were identified (0.1 hPa, roughly 64 km). Decisive findings revealed the processing of the unfiltered solar and H_2O data time series with wavelet coherence software. Intermittently occurring

correlations of up to 0.8 in the squared wavelet coherence analysis and high common wavelet power during April 2011 and March 2015 (the more active solar time period B) indicated that mesospheric H_2O oscillations are closely linked to the solar rotation cycle for a mid-latitudinal location, such as Bern.

The origin of the observed phase (time lag) variability between the water vapor time series of the microwave radiometer and solar data set is uncertain. An interaction with a 27-day recurrent geomagnetic activity could be considered, particularly during solar storms perturbations in the polar region are likely. As mentioned in the discussions (Section 6), the chemical lifetime of mesospheric water vapor is expected to contribute to the detected phase differences. In addition, the competition between photodissociation loss and advective transport processes of mesospheric H_2O may explain the sometimes variable phase relationship.

A more global view on the 27-day wave in mesospheric water has also been presented, showing that the largest variations at 0.04 hPa occur in the mid-latitudes and polar regions. Not only the local mean amplitude spectra (MIAWARA and MLS) show an enhancement in the 27-day band during the investigated higher solar activity period, but also the mean amplitude spectra of the zonal mean MLS measurements around the latitude circle of the location of MIAWARA (Bern).

To better understand the impact of gravity waves on mesospheric water above the alpine region, which is poorly understood, we plan new investigations in the future that make use of numerical simulations in conjunction with ground-based observations. For example EULAG (Smolarkiewicz and Margolin, 1997), a numerical solver for all scale geophysical flows, is well suited to simulate deep propagating gravity waves into the mesosphere.

Other follow-up studies, involving coupled dynamic-photochemistry modeling in the middle atmosphere, could be performed in the future for comparison with measured trace gas variations, such as water vapor, by existing ground-based instrument networks like NDACC. A reference to existing and convenient 3-dimensional numerical models like HAMMONIA shall be noted and further studies are encouraged.

Summarizing, our study showed that

- enhanced H_2O wave activity above 0.1 hPa in the 27-day band is present during the more active time of solar cycle 24 (period B from 2011-04-01 to 2015-03-31), not only locally for Bern but also at other places in the 44–50°N latitude belt (Fig. 6);
- absolute H_2O wave amplitudes at periods above 20 days compare well between Aura MLS and MIAWARA in temporal mean spectra;
- northern hemispheric H_2O wave amplitudes in the 27-day period band (0.04 hPa pressure level) have pronounced horizontal structures and mid-latitudinal/polar regions show larger areas of higher H_2O oscillations compared to the subtropics/tropics;
- relative H_2O wave amplitudes in the 27-day band frequently exceed 10% and amplifying processes accompanied by the solar forcing (recurrent geomagnetic activity or periodic-advective transport by atmospheric waves) should be taken into account;
- negative cross-correlation up to −0.3 to −0.4 between solar Lyman-α and MIAWARA H_2O have been identified (confidence level: ≥99%) at 0.03 hPa associated with a response phase lag of roughly 6–10 days during the more active Lyman-α oscillation period B (2011-04-01 to 2015-03-31);
- significant (95% confidence interval) high common wavelet power during intensifying sunspot activity exists;
- domains in time-frequency space with high correlations (>0.8) appear sporadic with variable phase lock behavior;
- after the solar superstorm event in July 2012 unusual high Lyman-α oscillations seem to induce anti-correlated oscillations in mesospheric H_2O VMR (0.011 − 0.1 hPa), which is discernible in the pressure averaged data series of MIAWARA.

The community of coupled dynamic-photochemistry modeling could benefit from our obtained results, for instance by performing model validations. Broader analyses of mid and high latitude atmospheric observations of ground- and space-based origin, in relation to different kind of atmospheric waves are still needed to better understand solar–terrestrial interactions.

Acknowledgments

This study has been carried out at the Institute of Applied Physics at the University of Bern, Bern, Switzerland. The Swiss National Science Foundation (SNF) provided funding under Grant number 200020-160048. Data access via the Interactive Solar IRradiance Data Center (LISIRD) is highly appreciated. In addition, we acknowledge A. Grinsted for providing XWT (cross-wavelet) and WTC (wavelet coherence) software as well as NASA for access to EOS Aura MLS data. Support by MeteoSwiss in the frame of GAW is appreciated.

References

Anderson, D.E., Cahalan, R.F., 2005. The Solar Radiation and Climate Experiment (SORCE) mission for the NASA Earth Observing System (EOS). Sol. Phys. 230, 3–6. http://dx.doi.org/10.1007/s11207-005-1592-6.

Bendat, J.S., Piersol, A.G., 2000. Random data analysis and measurement procedures. Meas. Sci. Technol. 11, 1825. http://dx.doi.org/10.1088/0957-0233/11/12/702.

Brasseur, G., Solomon, S., 2006. Aeronomy of the Middle Atmosphere: Chemistry and Physics of the Stratosphere and Mesosphere vol. 32. Springer.

Carrington, R.C., 1859. Description of a singular appearance seen in the Sun on September 1, 1859. Mon. Not. R. Astron. Soc. 20, 13–15. http://dx.doi.org/10.1093/mnras/20.1.13.

Chabrillat, S., Kockarts, G., 1997. Simple parameterization of the absorption of the solar Lyman-alpha line. Geophys. Res. Lett. 24, 2659–2662. http://dx.doi.org/10.1029/97GL52690.

Chapman, S., 1930. A theory of upper-atmospheric ozone. Memoirs R. Meteorol. Soc. 3, 103–125.

Deuber, B., Haefele, A., Feist, D.G., Martin, L., Kämpfer, N., Nedoluha, G.E., Yushkov, V., Khaykin, S., Kivi, R., Vomel, H., 2005. Middle Atmospheric Water Vapour Radiometer – MIAWARA: validation and first results of the LAUTLOS/WAVVAP campaign. J. Geophys. Res. 110, D13306. http://dx.doi.org/10.1029/2004JD005543.

Eriksson, P., Buehler, S., Davis, C., Emde, C., Lemke, O., 2011. ARTS, the atmospheric radiative transfer simulator, version 2. J. Quant. Spectrosc. Radiat. Transf. 112, 1551–1558. http://dx.doi.org/10.1016/j.jqsrt.2011.03.001.

Eriksson, P., Jiménez, C., Buehler, S.A., 2005. Qpack, a general tool for instrument simulation and retrieval work. J. Quant. Spectrosc. Radiat. Transf. 91, 47–64. http://dx.doi.org/10.1016/j.jqsrt.2004.05.050.

Espy, P.J., Hibbins, R.E., Riggin, D.M., Fritts, D.C., 2005. Mesospheric planetary waves over Antarctica during 2002. Geophys. Res. Lett. 32, L21804. http://dx.doi.org/10.1029/2005GL023886.

Fytterer, T., Santee, M.L., Sinnhuber, M., Wang, S., 2015. The 27-day solar rotational effect on mesospheric nighttime oh and o3 observations induced by geomagnetic activity. J. Geophys. Res. Space Physics 120, 7926–7936. http://dx.doi.org/10.1002/2015JA021183.

Grinsted, A., Moore, J.C., Jevrejeva, S., 2004. Application of the cross wavelet transform and wavelet coherence to geophysical time series. Nonlinear Process. Geophys. 11, 561–566. http://dx.doi.org/10.5194/npg-11-561-2004.

Gruzdev, A., Schmidt, H., Brasseur, G., 2009. The effect of the solar rotational irradiance variation on the middle and upper atmosphere calculated by a three-dimensional chemistry-climate model. Atmos. Chem. Phys. 9, 595–614. http://dx.doi.org/10.5194/acp-9-595-2009.

Holton, J.R., Hakim, G.J., 2013. An Introduction to Dynamic Meteorology. Academic Press, Boston.

Hood, L.L., 2013. Effects of Solar UV Variability on the Stratosphere. American Geophysical Union, Washington, DC, pp. 283–303. http://dx.doi.org/10.1029/141GM20.

Jevrejeva, S., Moore, J., Woodworth, P., Grinsted, A., 2005. Influence of large-scale atmospheric circulation on European sea level: results based on the wavelet transform method. Tellus A 57, 183–193. http://dx.doi.org/10.1111/j.1600-0870.2005.00090.x.

Kämpfer, N., Nedoluha, G., Haefele, A., De Wachter, E., 2012. Microwave Radiometry.

ISSI Scientific Report Series. vol. 10. Springer, New York. http://dx.doi.org/10.1007/978-1-4614-3909-7.
Khosravi, R., Brasseur, G., Smith, A., Rusch, D., Walters, S., Chabrillat, S., Kockarts, G., 2002. Response of the mesosphere to human-induced perturbations and solar variability calculated by a 2-d model. J. Geophys. Res. 107. http://dx.doi.org/10.1029/2001JD001235, ACH 7-1-ACH 7-21.
Krivolutsky, A., Kiryushov, V., Vargin, P., 2003. Generation of wave motions in the middle atmosphere induced by variations of the solar ultraviolet radiation flux (based on UARS satellite data). Int. J. Geomagn. Aeron. 3, 267–279.
Liu, Y.D., Luhmann, J.G., Kajdič, P., Kilpua, E.K.J., Lugaz, N., Nitta, N.V., Möstl, C., Lavraud, B., Bale, S.D., Farrugia, C.J., Galvin, A.B., 2014. Observations of an extreme storm in interplanetary space caused by successive coronal mass ejections. Nat. Commun., 5. http://dx.doi.org/10.1038/ncomms4481.
Livesey, N.J., Read, W.G., Wagner, P.A., Froidevaux, L., Lambert, A., Manney, G.L., Millán Valle, L.F., Pumphrey, H.C., Santee, M.L., Schwartz, M.J., Wang, S., Fuller, R. A., Jarnot, R.F., Knosp, B.W., Martinez, E., 2015. Version 4.2x Level 2 Data Quality and Description Document. Technical Report. Jet Propulsion Laboratory, California Institute of Technology.
Mayr, H., Mengel, J., Huang, F., Nash, E., 2009. Intra-seasonal monthly oscillations in stratospheric NCEP data and model results. J. Atmos. Sol. Terr. Phys. 71, 1299–1308. http://dx.doi.org/10.1016/j.jastp.2009.05.003.
McClintock, W.E., Rottman, G.J., Woods, T.N., 2000. Solar Stellar Irradiance Comparison Experiment II (SOLSTICE II) for the NASA Earth Observing system's solar radiation and climate experiment mission, Proc. SPIE 4135, 225–234. http://dx.doi.org/10.1117/12.494220.
McCormack, J.P., Hoppel, K.W., Siskind, D.E., 2008. Parameterization of middle atmospheric water vapor photochemistry for high-altitude nwp and data assimilation. Atmos. Chem. Phys. 8, 7519–7532. http://dx.doi.org/10.5194/acp-8-7519-2008.
McDonald, A.J., Hibbins, R.E., Jarvis, M.J., 2011. Properties of the quasi 16 day wave derived from EOSMLS observations. J. Geophys. Res. 116, D06112. http://dx.doi.org/10.1029/2010JD014719.
Oppenheim, A.V., Schafer, R.W., Buck, J.R., et al., 1989. Discrete-Time Signal Processing volume 2. Prentice-Hall, Englewood Cliffs.
Riggin, D.M., Liu, H.L., Lieberman, R.S., Roble, R.G., III, J.M.R., Mertens, C.J., Mlynczak, M.G., Pancheva, D., Franke, S.J., Murayama, Y., Manson, A.H., Meek, C.E., Vincent, R.A., 2006. Observations of the 5-day wave in the mesosphere and lower thermosphere. J. Atmos. Sol. Terr. Phys. 68, 323–339. http://dx.doi.org/10.1016/j.jastp.2005.05.010.
Rodgers, C.D., 2000. Inverse Methods for Atmospheric Sounding: Theory and Practice vol. 2. World Scientific Publishing Co Pte. Ltd..
Rottman, G., 2005. The SORCEMission, in: Rottman, G., Woods, T., George, V. (Eds.), The Solar Radiation and Climate Experiment (SORCE). Springer, New York, pp. 7–25. http://dx.doi.org/10.1007/0-387-37625-9_2.
Ruzmaikin, A., Lee, J.N., Wu, D.L., 2014. Patterns of carbon monoxide in the middle atmosphere and effects of solar variability. Adv. Sp. Res. 54, 320–326. http://dx.doi.org/10.1016/j.asr.2013.06.033.
Salby, M.L., 1981. The 2-day wave in the middle atmosphere: observations and theory. J. Geophys. Res. 86, 9654–9660. http://dx.doi.org/10.1029/JC086iC10p09654.
Scheiben, D., Tschanz, B., Hocke, K., Kämpfer, N., Ka, S., Oh, J.J., 2014. The quasi 16-day wave in mesospheric water vapor during boreal winter 2011/2012. Atmos. Chem. Phys. 14, 6511–6522. http://dx.doi.org/10.5194/acp-14-6511-2014.
Schmidt, H., Brasseur, G., Charron, M., Manzini, E., Giorgetta, M., Diehl, T., Fomichev, V., Kinnison, D., Marsh, D., Walters, S., 2006. The HAMMONIA chemistry climate model: sensitivity of the mesopause region to the 11-year solar cycle and CO_2 doubling. J. Clim. 19, 3903–3931. http://dx.doi.org/10.1175/JCLI3829.1.
Shapiro, A.V., Rozanov, E., Shapiro, A.I., Wang, S., Egorova, T., Schmutz, W., Peter, T., 2012. Signature of the 27-day solar rotation cycle in mesospheric OH and H_2O observed by the Aura Microwave Limb Sounder. Atmos. Chem. Phys. 12, 3181–3188. http://dx.doi.org/10.5194/acp-12-3181-2012.
Smolarkiewicz, P.K., Margolin, L.G., 1997. On forward-in-time differencing for fluids: an Eulerian/semi-Lagrangian non-hydrostatic model for stratified flows. Atmos. Ocean 35, 127–152.
Stief, L., Donn, B., Glicker, S., Gentieu, E., Mentall, J., 1972. Photochemistry and lifetimes of interstellar molecules. Astrophys. J. 171, 21. http://dx.doi.org/10.5194/acp-12-3181-2012.
Studer, S., Hocke, K., Kämpfer, N., 2012. Intraseasonal oscillations of stratospheric ozone above Switzerland. J. Atmos. Sol. Terr. Phys. 74, 189–198. http://dx.doi.org/10.1016/j.jastp.2011.10.020.
Thomas, G.E., 1996. Global change in the mesosphere-lower thermosphere region: has it already arrived?. J. Atmos. Terr. Phys. 58, 1629–1656. http://dx.doi.org/10.1016/0021-9169(96)00008-6.
Torrence, C., Compo, G.P., 1998. A practical guide to wavelet analysis. Bull. Am. Meteor. Soc. 79, 61–78. http://dx.doi.org/10.1175/1520-0477(1998)079⟨0061:APGTWA⟩2.0.CO;2.
Vardavas, I., Carver, J., Taylor, F., 1998. The role of water-vapour photodissociation on the formation of a deep minimum in mesopause ozone. Ann. Geophys. 16, 189–196. http://dx.doi.org/10.1007/s00585-998-0189-4.
Wang, B., Wang, Y., 1996. Temporal structure of the Southern oscillation as revealed by waveform and wavelet analysis. J. Clim. 9, 1586–1598. http://dx.doi.org/10.1175/JCLI-D-12-00345.1.
Welch, P., 1967. The use of fast Fourier transform for the estimation of power spectra: a method based on time averaging over short, modified periodograms. IEEE Trans. Audio Electroacoust., 70–73. http://dx.doi.org/10.1109/TAU.1967.1161901.
Weron, R., 2007. Modeling and forecasting electricity loads and prices: a statistical approach vol. 403. John Wiley & Sons, Chichester.
Williams, V., Austin, J., Haigh, J., 2001. Model simulations of the impact of the 27-day solar rotation period on stratospheric ozone and temperature. Adv. Sp. Res. 27, 1933–1942. http://dx.doi.org/10.1016/S0273-1177(01)00263-0.
Woods, T.N., Bailey, S.M., Eparvier, F.G., Lawrence, G.M., Lean, J., McClintock, W.E., Roble, R.G., Rottman, G.J., Solomon, S.C., Tobiska, W.K., Ucker, G.J., White, O.R., 1998. TIMED Solar EUV Experiment. Proc. SPIE 3442, 180–191. http://dx.doi.org/10.1117/12.330255.
Woods, T.N., Tobiska, W.K., Rottman, G.J., Worden, J.R., 2000. Improved solar Lyman α irradiance modeling from 1947 through 1999 based on UARS observations. J. Geophys. Res. 105, 27195–27215. http://dx.doi.org/10.1029/2000JA000051.
Wu, D.L., Hays, P.B., Skinner, W.R., 1994. Observations of the 5-day wave in the mesosphere and lower thermosphere. Geophys. Res. Lett. 21, 2733–2736. http://dx.doi.org/10.1029/94GL02660.
Wu, D.L., Jiang, J.H., 2005. Interannual and seasonal variations of diurnal tide, gravity wave, ozone, and water vapor as observed by MLS during 1991–1994. Adv. Sp. Res. 35, 1999–2004. http://dx.doi.org/10.1016/j.asr.2004.12.018.
Yue, J., Liu, H.L., Chang, L.C., 2012. Numerical investigation of the quasi 2 day wave in the mesosphere and lower thermosphere. J.Geophys. Res.: Atmos. 117, D05111. http://dx.doi.org/10.1029/2011JD016574.
Zhang, Q., Xu Yu, C., Jiang, T., Wu, Y., 2007. Possible influence of ENSO on annual maximum streamflow of the Yangtze River. China. J. Hydrol. 333, 265–274. http://dx.doi.org/10.1016/j.jhydrol.2006.08.010.